International Geology Review

ISSN: (Print) (Online) Journal homepage: https://www.tandfonline.com/loi/tigr20

A new perspective on Cenozoic calc-alkaline and shoshonitic volcanic rocks, eastern Saveh (central Iran)

Fatemeh Nouri, Hossein Azizi, Yoshihiro Asahara & Robert J. Stern

To cite this article: Fatemeh Nouri, Hossein Azizi, Yoshihiro Asahara & Robert J. Stern (2021) A new perspective on Cenozoic calc-alkaline and shoshonitic volcanic rocks, eastern Saveh (central Iran), International Geology Review, 63:4, 476-503, DOI: 10.1080/00206814.2020.1718005

To link to this article: https://doi.org/10.1080/00206814.2020.1718005

Published online: 28 Jan 2020.

INTERNATIONAL GEOLOGY REVIEW
2021, VOL. 63, NO. 4, 476–503
https://doi.org/10.1080/00206814.2020.1718005

Taylor & Francis
Taylor & Francis Group

ARTICLE

A new perspective on Cenozoic calc-alkaline and shoshonitic volcanic rocks, eastern Saveh (central Iran)

Fatemeh Nouri[a], Hossein Azizi[a], Yoshihiro Asahara[b] and Robert J. Stern[c]

[a]Department of Mining Engineering, Faculty of Engineering, University of Kurdistan, Sanandaj, Iran; [b]Department of Earth and Environmental Sciences, Graduate School of Environmental Studies, Nagoya University, Nagoya, Japan; [c]Geosciences Department, University of Texas at Dallas, Richardson, TX, USA

ABSTRACT

Late Eocene – Oligocene volcanic rocks in the eastern Saveh region of the Urumieh-Dokhtar magmatic arc (UDMA) are representative of Paleogene magmatic activity in Iran. They show a wide range of silica-undersaturated to silica-oversaturated compositions, from basalt-trachy basalt and tephri-phonolite to trachyte-latite. Whole rock chemical compositions define a continuous assemblage of mafic and felsic rocks in terms of SiO_2 (46.3 to 71.1 wt.%), Al_2O_3 (12.5–19.2 wt.%), K_2O (2.06–12.23 wt.%) and TiO_2 (0.41–1.75 wt.%) contents, Mg number (6.8–51) and K_2O/Na_2O ratios (0.53–30.2). Abundances of rare earth elements in the tephri-phonolite group are much higher than in the trachyte-latite and basalt-trachy basalt groups. Elevated contents of large ion lithophile elements such as Ba (191–7311 ppm) and Pb (6.49–118 ppm) as well as depletions in high field strength elements such as Nb (2.43–40.6 ppm), Ta (0.15–2.24 ppm), Zr (40.8–258 ppm) and TiO_2 (0.40–1.77 wt.%) characterize these rocks. Initial ratios of $^{87}Sr/^{86}Sr$ from 0.7046 to 0.7074 and $\varepsilon_{Nd}(t)$ from +0.9 to +3.3 show that these were derived from parental magma extracted from partial melting of metasomatized mantle, namely amphibole- and/or phlogopite-bearing peridotite. Fractionation of feldspar, clinopyroxene, amphibole and phlogopite, and minor contamination with upper crust was responsible for the large variation of the rock types observed. We explain contemporaneous late Eocene – Oligocene calc-alkaline and high-K magmatic activity in the UDMA as due to the partial melting of both hot metasomatized asthenospheric and subcontinental lithospheric mantle in an extensional tectonic regime. This extensional regime probably developed due to the rollback of the subducted Neo-Tethys oceanic plate.

ARTICLE HISTORY
Received 7 September 2019
Accepted 11 January 2020

KEYWORDS
Mantle metasomatism; shoshonitic rocks; highly potassic rocks; Urumieh-Dokhtar magmatic belt; Neo-Tethys subduction; slab rollback

1. Introduction

The Zagros orgen of Iran is part of the Alpine-Himalayan orogenic belt and has been affected by N-dipping subduction of the Neo-Tethys Ocean beginning in the Mesozoic (e.g. Stöcklin 1968; Berberian and Berberian 1981; Ghasemi and Talbot 2006; Azizi and Stern 2019). The Zagros orogenic belt consists of three parallel tectonic zones (Figure 1) (Alavi 2004): (1) Zagros fold-and-thrust belt, (2) Sanandaj-Sirjan zone, and (3) Urumieh-Dokhtar magmatic assemblage (UDMA). As the subduction zone and the overlying continental magmatic arc matured, igneous activity produced a broad belt of mostly Cenozoic volcanic and plutonic rocks of the UDMA (Figure 1, Table 1) which forms a distinct, linear intrusive-extrusive complex (Stöcklin 1968; Berberian and Berberian 1981; Ghasemi and Talbot 2006; Omrani *et al*. 2008; Verdel *et al*. 2011; Chiu *et al*. 2013) located between the Sanandaj-Sirjan zone in the southwest and Central Iran in the northeast (Figure 1).

The UDMA (Figure 1) emplaced and erupted a wide range of igneous rocks from calc alkaline to alkaline and shoshonitic (Amidi *et al*. 1984; Hassanzadeh 1993; Omrani *et al*. 2008; Ahmadzadeh *et al*. 2010; Rezaei-Kahkhaei *et al*. 2011; Verdel *et al*. 2011; Sarjoughian *et al*. 2012; Chiu *et al*. 2013; Pang *et al*. 2013; Yazdani *et al*. 2018). Different scenarios have been suggested for the UDMA geodynamic evolution. Amidi *et al*. (1984) proposed a rift model, whereas the most other models consider the UDMA as a continental arc (Berberian and Berberian 1981) or island arc (Alavi 1994). Ghasemi and Talbot (2006) proposed a post-collision origin for late to middle Eocene volcanic rocks in this belt, but this is not supported because collision with Arabia began in Oligocene-Miocene time. There is now consensus that the UDMA marks the magmatic front of the Late Cretaceous and younger continental arc of Iran. Verdel *et al*. (2011) emphasized Palaeogene magmatism and extension as a result of slab retreat or slab rollback following a Cretaceous episode of flat slab subduction.

CONTACT Fatemeh Nouri f.nourisandiani@gmail.com Department of Mining Engineering, Faculty of Engineering, University of Kurdistan, Sanandaj, Iran

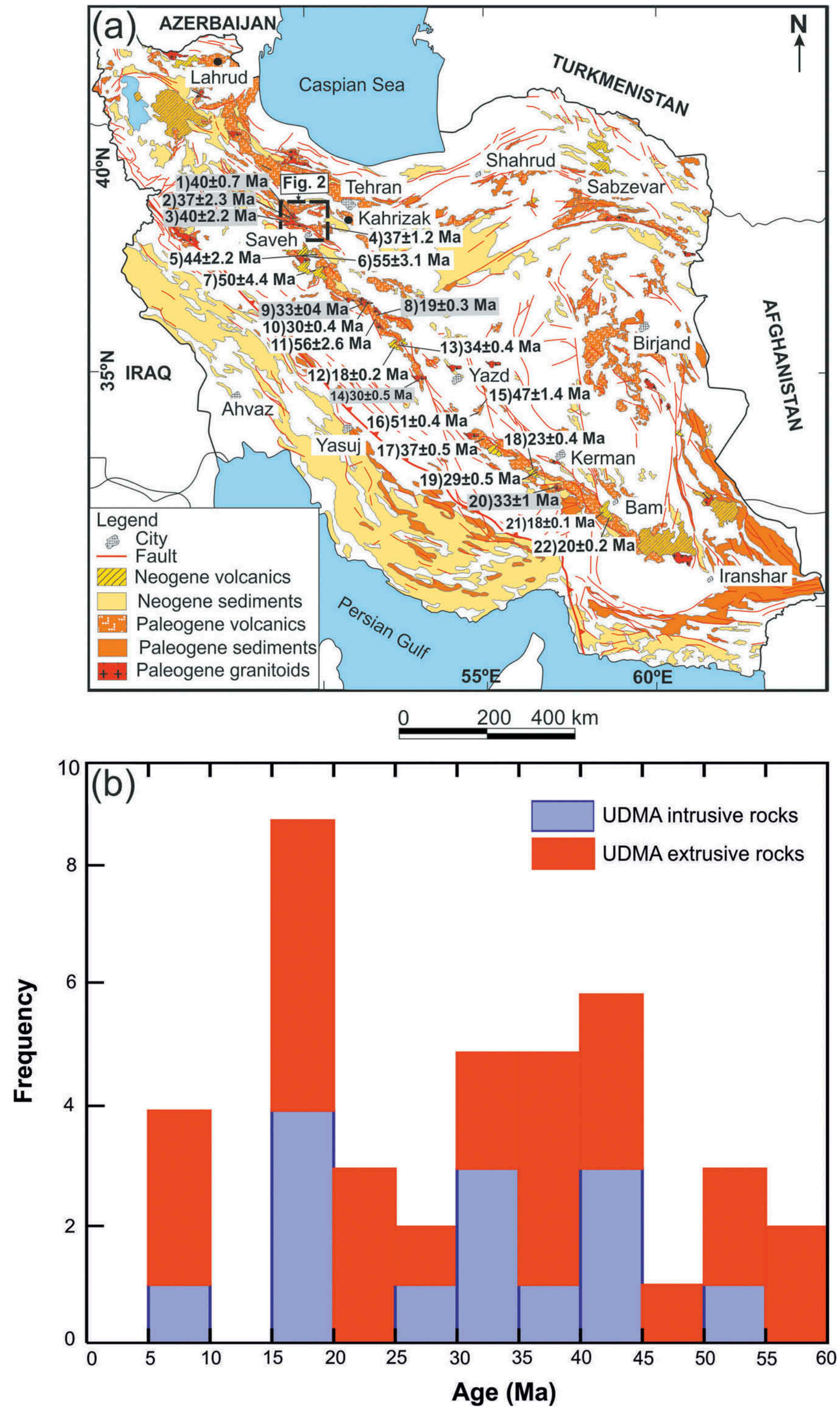

Figure 1. (a) Simplified geological map of Iran (modified from Stöcklin 1968), showing the distribution of Cenozoic igneous rocks and the location of Figure 2. (b) Histogram of radiometric ages for UDMA volcanic and plutonic rocks, source data for UDMA intrusive and volcanic ages are from Table 1.

An interesting aspect of Palaeogene UDMA igneous activity is the presence of alkaline igneous rocks. Alkaline volcanic rocks contain high concentrations of large ion lithophile and trace elements, and these abundances are mostly explained by low degrees of partial melting and unusual mineralogy of the mantle source (Conticelli *et al*. 2009; Prelević *et al*. 2010; Huang and Hou 2017; Sokol *et al*. 2019). They make up less than 1% of all continental igneous rocks (Gill 2011). Alkaline igneous rocks are often found behind the magmatic front of convergent

Table 1. The ages of extrusive and intrusive bodies enter the UDMA from Saveh to south.

Area	Number(Figure 1)	Rock type	Age (Ma)	Method	Latitude	Longitude	References
Saveh	1	Granite	40 ± 0.7 Ma	U-Pb	35° 32´	48° 50´	Kazemi *et al.* (2019)
	2	Granite	37 ± 2.3 Ma	U-Pb	35° 06´	50° 08´	Nouri *et al.* (2018)
	3	Diorite	40 ± 2.2 Ma	U-Pb	35° 10´	50° 10´	Nouri *et al.* (2018)
	4	Tuff	37 ± 1.2 Ma	U-Pb	35° 26´	50° 09´	Verdel *et al.* (2011)
Tafresh	5	Tuff	44 ± 2.2 Ma	Ar-Ar	34° 32´	50° 07´	Verdel *et al.* (2011)
	6	Andesite	55 ± 3.1 Ma	Ar-Ar	34° 53´	50° 12´	Verdel *et al.* (2011)
	7	Volcanic	50 ± 4.4 Ma	Ar-Ar	34° 55´	50° 20´	Verdel *et al.* (2011)
Kashan	8	Diorite	33 ± 0.3 Ma	U-Pb	33° 43´	51° 29´	Chiu *et al.* (2013)
Natanz	9	Granite	19 ± 0.3 Ma	U-Pb	33° 36´	51° 50´	Chiu *et al.* (2013)
	10	Andesite	30 ± 0.4 Ma	U-Pb	33° 30´	51° 51´	Chiu *et al.* (2013)
	11	Basalt	56 ± 2.6 Ma	U-Pb	33° 21´	51° 52´	Chiu *et al.* (2013)
	12	Rhyolite	37 ± 0.4 Ma	U-Pb	32° 44´	52° 52´	Chiu *et al.* (2013)
	13	Andesite	34 ± 0.4 Ma	U-Pb	32° 45´	52° 56´	Chiu *et al.* (2013)
Yazd	14	Andesite	42 ± 0.4 Ma	U-Pb	32° 20´	53° 50´	Chiu *et al.* (2013)
	15	Andesite	47 ± 1.4 Ma	U-Pb	31° 31´	54° 26´	Chiu *et al.* (2013)
	16	Andesite	51 ± 0.4 Ma	U-Pb	31° 18´	54° 16´	Chiu *et al.* (2013)
Kerman	17	Andesite	37 ± 0.5 Ma	U-Pb	30° 35´	55° 42´	Chiu *et al.* (2013)
	18	Andesite	23 ± 0.4 Ma	U-Pb	29° 37´	56° 42´	Chiu *et al.* (2013)
	19	Basalt	29 ± 0.5 Ma	U-Pb	29° 55´	56° 58´	Chiu *et al.* (2013)
	20	Basalt	18 ± 0.1 Ma	U-Pb	29° 39´	56° 45´	Chiu *et al.* (2013)
	21	Rhyolite	18 ± 0.1 Ma	U-Pb	29° 01´	57° 54´	Chiu *et al.* (2013)
	22	Basalt	20 ± 0.2 Ma	U-Pb	28° 51´	57° 51´	Chiu *et al.* (2013)

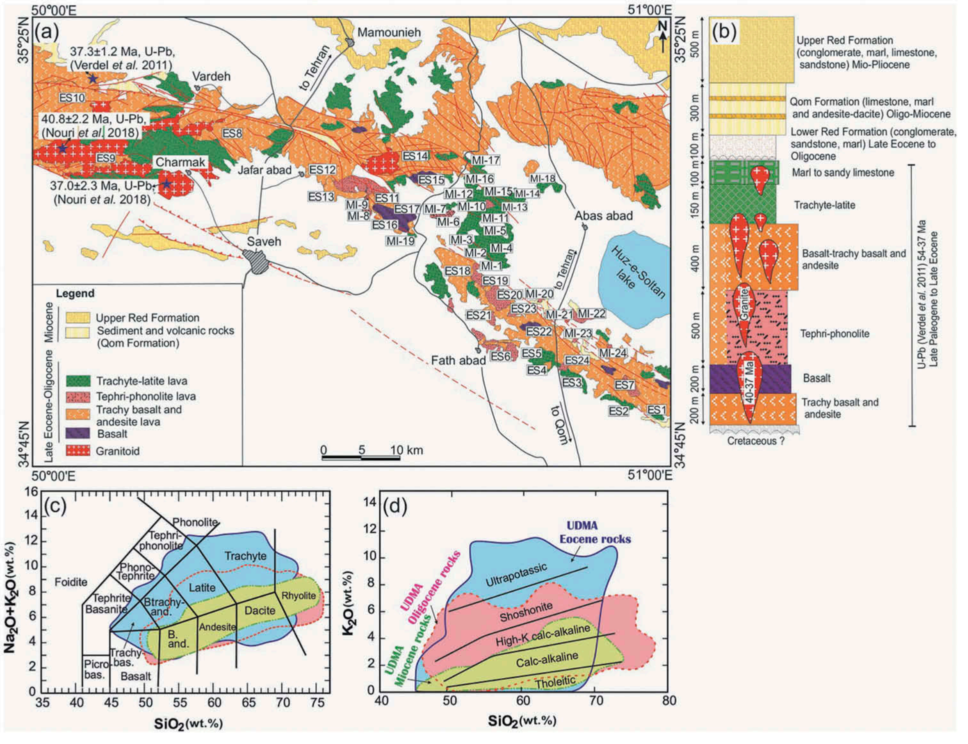

Figure 2. (a) Simplified geological map of the UDMA and related units around Saveh. Saveh map from Ghalamghash (1998), Zaviyeh map from Amidi *et al.* (2004); Qom map from Zamanni and Hossaini (1999). (b) Simplified stratigraphic section of igneous and sedimentary rocks in the Saveh area showing the stratigraphic occurrence of three groups studied here: basalt-trachy basalt, trachyte-latite, and tephri-phonolite. (c, d) Simplified TAS (Le Maitre 1989) and magmatic series (Ewart, 1982) diagrams for igneous rocks of the UDMA (source data from Tutti *et al.* (2008), Omrani *et al.* (2008), Ahmadian *et al.* (2009, 2010), Torabi (2009), Verdel *et al.* (2011), Etemadi *et al.* (2012), Ayati (2015), Delavari *et al.* (2017), Haghighi Bardineh *et al.* (2018), Kazemi *et al.* (2019), Nouri *et al.* (2018), Yazdani *et al.* (2018).

margins but they are unusual along the magmatic front (Walker 1981; Muñoz and Stern 1989; Yoshida 2001; Workman *et al.* 2004; Vogel *et al.* 2006, 2006; Pilet *et al.* 2008; Takahashi *et al.* 2012; Dai *et al.* 2018; Kepezhinskas *et al.* 2019), as represented by the UDMA. Instead, continental arc magmatic front igneous rocks are generally calc-alkaline. The presence of alkaline igneous rocks in the UDMA is very interesting in this regard.

Our target in this work is to better understand the geodynamic setting and petrogenesis of late Eocene to Oligocene potassic volcanic rocks in the middle of the UDMA. We present detailed petrological results along with 48 whole rock chemical analysis and Sr-Nd isotope ratios. This work was undertaken to better understand the geochemical and geodynamic evolution of the central UDMA and the contribution of diverse mantle sources, particularly the association between subduction-related and within-plate magmatism in the central UDMA. In addition, we developed a comprehensive petrogenetic model that is useful for understanding the volcanic history for late Eocene to Oligocene UDMA volcanism. Finally, we suggest a new model to show the relation of calc-alkaline and alkaline rocks which erupted at the same time and how differentiation and assimilation made an unusually large variety of magmas in the eastern Saveh segment of the UDMA.

2. Geological background

The UDMA is a NW-SE trending belt in Iran that consists of Eocene-Quaternary extrusive and intrusive igneous rocks and related volcanoclastic units (Figure 1). Volcanic rocks vary from mafic to felsic and were erupted in continental to shallow submarine environments (Berberian and King 1981; Verdel *et al*. 2011). The main magmatic activity in the ~900 km-long segment of the UDMA from Qom to Baft occurred in Eocene time, but continued into Neogene time (Omrani *et al*. 2008; Chiu *et al*. 2013). Extensive arc magmatism accompanied subduction of Neo-Tethys lithosphere beneath central Iran, with a major pulse during middle Eocene time, from 54 Ma to 37 Ma (Berberian and King 1981; Verdel *et al*. 2011; Chiu *et al*. 2013; Moghadam *et al*. 2015).

Evolution from an extensional to compressional arc happened during Eocene time and was associated with orogenic collapse (Berberian and King 1981; Verdel *et al*. 2011; Chiu *et al*. 2013; Moghadam *et al*. 2015). This was accompanied by extension and exhumation of metamorphic core complexes, especially in central Iran (Ramezani and Tucker 2003; Verdel *et al*. 2011). Palaeogene UDMA volcanic rocks are interbedded with marine and continental sedimentary rocks (Amidi *et al*. 1984; Verdel *et al*. 2011). Marine fossils such as *Nummulites fabiani, bryozoan, coral and Morozovella sp.* show that UDMA volcanic sequences were deposited in a shallow marine basin, as expected for an extensional arc (Verdel *et al*. 2011). Eocene volcanic rocks are covered by terrigenous sediments of the late Eocene to early Oligocene Lower Red Formation, including conglomerate, sandstone, shale, and gypsum. Eocene volcanic rocks are mostly calc-alkaline and evolved to alkaline and high K-alkaline suites in the late Eocene (Amidi *et al*. 1984; Hassanzadeh 1993), sometimes to shoshonite (Sarjoughian *et al*. 2012) and adakite (Omrani *et al*. 2008; Yazdani *et al*. 2018; Kazemi *et al*. 2019). Yazdani *et al*. (2018) inferred that asthenospheric upwelling related to slab rollback led to Eocene calc-alkaline and shoshonitic volcanism and that the magma source was metasomatized subcontinental lithospheric mantle. Oligocene magmatism shifted to OIB-like (Verdel *et al*. 2011). Verdel *et al*. (2011) suggested that asthenospheric upwelling related to slab rollback led to Oligocene-Miocene volcanism. However, Ayati (2015) concluded that Mio-Pliocene volcanic to subvolcanic bodies in the Salafchegan region were derived from enriched lithospheric mantle and these melts were subsequently modified by assimilation and fractional crystallization. Qom Formation marine limestones and marls (late Oligocene to early Miocene) conformably overly Oligocene volcanic rocks. Pliocene and Quaternary UDMA igneous rocks consist of alkaline lava flows and pyroclastics (Berberian and Berberian 1981; Jahangiri 2007; Omrani *et al*. 2008; Ahmadzadeh *et al*. 2010). Lithospheric delamination beneath over-thickened Iranian crust (Hatzfeld and Molnar 2010) or breakoff of the Neo-Tethys slab (Omrani *et al*. 2008) may have led to Pliocene-Quaternary UDMA igneous activity.

Eocene to Oligocene volcanic rocks in the eastern Saveh area (Figure 2) are part of the central UDMA. Erosion here has cut into and exposed deeper parts of the UDMA succession. Several plutonic bodies (Khalkhab-Neshveh and Selijerd granitoids), with U-Pb age of 40–37 Ma (Nouri *et al*. 2018) intruded the volcano-sedimentary rocks, consisting of gabbro, diorite, quartz monzonite, and granite (Caillat *et al*. 1978; Rezaei-Kahkhaei *et al*. 2011; Nouri *et al*. 2018; Kazemi *et al*. 2019).

The main igneous rock outcrops in the eastern Saveh area are late Eocene to early Oligocene in age, including volcanics with interbedded sedimentary rocks and grantoids, all of which were affected by strike-slip faulting (Ghasemi and Talbot 2006; Verdel *et al*. 2011; Chiu *et al*. 2013).

3. Field description and observations

Late Eocene to Oligocene volcanic rocks in the eastern Saveh area (Figures 2 and 3(a-c)) are well exposed and are interbedded with sedimentary layers such as limestone, shale, sandstone, and conglomerate (Figure 3(d,e)). The sandstones are generally grey to black in colour and are interbedded with volcanic rocks and limestone and sandly limestone, indicating a marine depositional environment. The entire volcanosedimentary complex has been deformed. Based on stratigraphic relationship and fossils

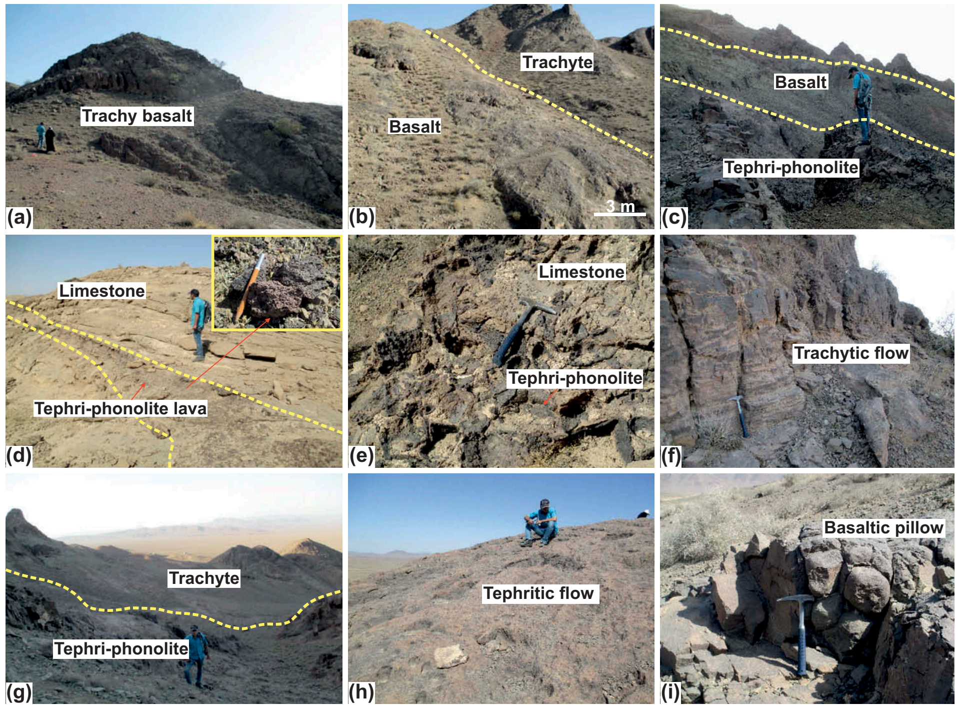

Figure 3. Photographs of various rocks in the study area. (a, b, c) Outcrops of trachyte, trachy basalt, and tephri-phonolite. (d) Limestone and sandy shale interbedded with tephri-phonolite. (e) Some tephri-phonolite patches and bombs in marine limestone. (f, g, h) Outcrops of trachyte, and tephri-phonolite lava flow. (i) Outcrop of mafic pillow lava.

such as *Lochartin sp., Nummulites sp., Asslina sp., Operculina sp., and Milliloids*, Amidi *et al*. (1984), Zamanni and Hossaini (1999) and Ghalamghash (1998) suggested a late Eocene to early Oligocene age for volcano-sedimentary rocks from the eastern Saveh area. Verdel *et al*. (2011) reported 56–37 Ma for volcanic sequences from northeast Saveh (37.3 Ma U-Pb zircon age: for tuffs from the upper part of the volcanic section and 56.6 to 44.3 Ma for volcanic rocks from the base to middle part). Volcanic rocks comprise basaltic, andesitic and trachy-basaltic lava flows, trachyte, tephri-phonolite, ignimbrite (Figure 3(c,f–h)), breccia, and their pyroclastic equivalents (Figure 3(g)). Figure 2(b) shows how the three groups occur in the ~ 1.5-km thick Eocene volcanic sequence around Saveh: basalt-trachybasalt is found at top and bottom, trachyte-latite is found in the lower half of the sequence, and tephri-phonolite is found in the middle of the section. All three groups are interbedded with shallow marine sediments.

Some mafic lavas show pillow structures (Figure 3(i)). Pillowed basalts are closely packed with lobes that closely fit with each other. Pillowed basaltic rocks are brecciated and sometimes oxidized red. Some tephri-phonolite patches and bombs are found in sediments (Figure 3(e)), indicating that Eocene UDMA volcanoes erupted in the sea. The rocks are affected by low-grade metamorphism, ranging from relatively undeformed basalt to greenstone, with some rocks having the typical chlorite and epidote assemblages characteristic of low-grade alteration.

4. Analytical techniques

All samples for whole rock geochemistry analysis were crushed using an agate mill. The major element contents of whole rocks were determined by conventional X-ray fluorescence (XRF) techniques using a Rigaku ZSX Primus II at Nagoya University (mixture of 0.5 g sample powder and 5.0 g lithium tetraborate). The mixture was melted at 1200°C for 12–17 min with a high-frequency bead sampler. Loss on ignition (LOI) was calculated by the weight difference after ignition at 950°C.

To determine the trace element abundances including rare earth elements (REEs) and Sr-Nd isotope ratios, 100 mg of the powdered sample was completely dissolved in 3 ml of HF (38%) and 0.5 to 1 ml of $HClO_4$ (70%) in a covered PTFE beaker at 120–140°C on a hotplate in a clean room. The dissolved sample was then dried at 140°C on a hotplate beneath infrared lamps. After drying, >10 ml of 2–6 M HCl was added to the dried sample to dissolve it, and the sample solution was moved to a polypropylene centrifuge tube to separate the residue from the clear upper portion. The residue was moved into a smaller PTFE vessel and then treated with HF + $HClO_4$ in a steel-jacketed bomb to ensure its complete dissolution. After the second HF-decomposition, the dried sample was dissolved in 5–10 ml of 2.4 M HCl, and the resulting solution was used for analyses of the trace elements and isotopes. The concentrations of the trace elements were analysed by ICP-MS (Agilent 7700x) at Nagoya University.

The isotope ratios of Sr and Nd were determined by VG Sector 54–30 and GVI IsoProbe-T thermal ionization mass spectrometers (TIMS) at Nagoya University. Mass fractionation during measurement was corrected according to $^{86}Sr/^{88}Sr$ = 0.1194 and $^{146}Nd/^{144}Nd$ = 0.7219. The NBS-MSRT 987 and JNdi-1 standards (Tanaka *et al*. 2000) were adapted as the natural Sr and Nd isotope ratio standards, respectively.

5. Petrography

Petrographical and geochemical studies show that eastern Saveh lava flows and pyroclastic rocks range from basalt trachy-basalt and thephri-phonolite to trachyte-latite. The pyroclastic rocks include tuff and breccia and are widespread in the area. Below we have separated them according to whole rock and microscopic results:

5.1. *Basalt-trachy basalt*

The volcanic rocks commonly exhibit intersertal, microlitic porphyritic and porphyritic textures (Figure 4(a,b)). The main mineralogical composition of this group is clinopyroxene, olivine, plagioclase, and Fe-Ti oxide. Clinopyroxenes are abundant as anhedral to euhedral microphenocrysts with resorbed rims (Figure 4(b)), Davarpanah (2009) reported augite to diopside composition for Saveh volcanic rocks; similar results for pyroxene mineral composition were reported by Yazdani *et al.* (2018) from Kahrizak volcanics (NE of study are). Clinopyroxenes generally show clear cleavage and some parts are altered to tremolite and chlorite. Olivine occurs as subhedral to anhedral crystals (Figure 4(a)) with chrysolite to hyalosiderite composition (Yazdani *et al*. 2018). Plagioclases (bytownite to anorthite core and albite to andesine rim (Davarpanah 2009; Yazdani *et al*. 2018) are

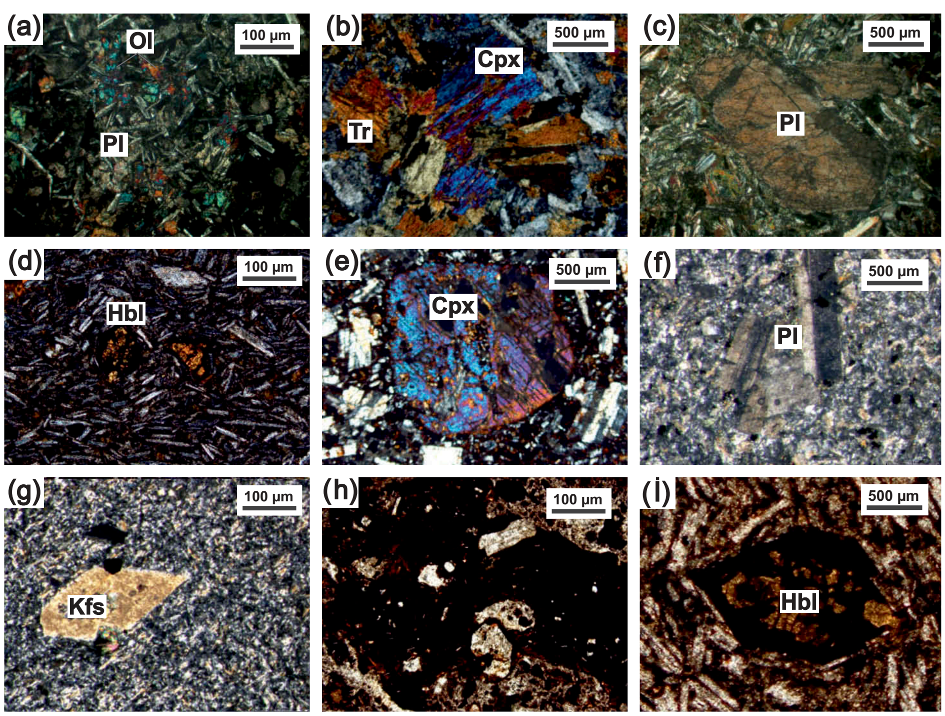

Figure 4. Photomicrographs of the eastern Saveh volcanic rocks. (a, b) Basalt-trachy basalt rocks commonly exhibit intersertal and glomeroporphyritic textures and consist of clinopyroxene, plagioclase, olivine, amphibole, and Fe-Ti oxide. (c) Plagioclase is generally subhedral to euhedral microphenocrysts and microlites with albite and polysynthetic twinning and are locally saussuritized. (d and e) Tephri-phonolites show porphyritic and glomeroporphyritic textures. Euhedral to subhedral clinopyroxene microphenocrysts generally show clear cleavage. (f-g) Both trachyte and latite usually show microgranular porphyritic and rarely trachytic textures with feldspar microphenocrysts. (h) latite with pyroclastic texture. (i) Most hornblendes are opacitized. Abbreviations: Ol= Olivine, Qtz= Quartz, Pl= Plagioclase, Hbl= Hornblende, Cpx= Clinopyroxene, Kfs= K-feldspar (Whitney and Evans 2010).

generally subhedral to euhedral microphenocrysts and microlites with albitic and polysynthetic twinning and are locally saussuritized (Figure 4(c)). Sometimes plagioclase surrounds clinopyroxene inclusions.

5.2. Tephri-phonolite

Tephri-phonolites show microgranular-porphyric, vitrophyric, and amygdaloidal textures. They consist of clinopyroxene, hornblende (Figure 4(d,e)), plagioclase, and K-feldspar. The groundmass of these rock is holocrystalline, composed of K-feldspar, clinopyroxene, and oxides. Euhedral to subhedral clinopyroxene microphenocrysts show clear cleavage (Figure 4(e)). Hornblendes (magnesio-hastengsite to magnesio hornblende (Davarpanah 2009; Yazdani *et al.* 2018) are euhedral to subhedral and are opacitized along their rims (Figure 4(d)). Carbonate, chlorite, and zeolite are secondary phases, Yazdani *et al.* (2014) based on the chemical composition of Kahrizak volcanics and zeolites suggested that volcanism and alteration occurred simultaneously in a submarine environment. The groundmass is composed of K-feldspar, plagioclase, clinopyroxene, and oxide minerals.

5.3. Trachyte-latite

Both trachyte and latite are dominated by feldspars and show trachytic and pyroclastic (Figure 4(g–i)) textures with feldspar microlites (Figure 4(f–i)). They consist of plagioclase, K-feldspar, hornblende, clinopyroxene, and Fe-Ti oxide. Euhedral to anhedral plagioclase occur as micropheonocrysts and microlites. K-feldspars (Figure 4(g)) are usually subhedral to euhedral and are sometimes poikilitic. Most hornblendes are opacitized (Figure 4(i)). Some hornblende are altered to chlorite and Fe-Ti oxide.

6. Results

6.1. Whole rock geochemistry

To examine the geochemistry and tectonic setting of the volcanic rocks in the study area, we integrate our results with published geochemical data for other Eocene K-rich volcanic sequences along the UDMA (Ahmadian *et al.* 2009; Tutti *et al.* 2008; Torabi 2009; Ahmadian *et al.* 2010; Etemadi *et al.* 2012; Yazdani *et al.* 2018).

Major oxides and trace element compositions of 48 whole rock samples are listed in Table 2. Eastern Saveh volcanic rocks are variably altered, as can be inferred from loss on ignition (LOI) values, which vary from 1.0 to 5.3 wt. % (Table 2). LOI reflects alteration of the glassy groundmass, presence of hydrous phases such as phlogopite and abundance of secondary minerals such as chlorite, clays, and zeolites (Yazdani *et al.* 2014; Yücel *et al.* 2017; Moghadam *et al.* 2018). Plots of Sr and Ba as a mobile element versus LOI (not shown) show that these elements do not vary with increasing LOI, although some tephri-phonolite samples show minor co-variation.

The total alkali versus silica (TAS) diagram (Le Maitre 1989) (Figure 5(a)) reveal three different groups: trachyte-latite, basalt-trachy basalt, and tephri-phonolite. Similarly, on the Nb/Y versus Zr/TiO_2 graph (Figure 5(b), Winchester and Floyd 1977), involving immobile elements the studied rocks range from sub-alkaline basalt to alkali basalt, andesite/basalt to rhyodacite/dacite and trachy andesite. Among the three groups, basalt-trachy basalts have the lowest SiO_2 contents (46.3 to 50.9 wt.%) and Na_2O+K_2O (4.24 to 9.56 wt.%) and highest MgO (2.2–5.80 wt.%) and Al_2O_3 (15.1–19.2 wt.%); because of geochemical differences, we divided these into two sub-groups of basalts and trachy basalts. Trachyte-latites have the highest SiO_2 contents (56.8 to 71.1 wt.%), intermediate Na_2O+K_2O (6.44 to 10.5 wt.%), lower MgO (0.08–1.51 wt.%) and lowest Al_2O_3 (13.2–15.6 wt.%). In contrast, the tephri-phonolites have intermediate SiO_2 (47.1 to 56.1 wt.%) and Al_2O_3 (12.5–17.6 wt.%), lower MgO (0.08–4.33 wt.%), and highest Na_2O+K_2O (9.56 to 12.8 wt.%). All three groups show low-moderate Cr (1.93–169 ppm) and Ni (2.38–61.8 ppm) (Table 2), suggesting they are fractionated.

In the K_2O versus Na_2O graph (Figure 5(c)), remarkable potash-sodium relations are seen, with K_2O/Na_2O ratios that vary from 10 to 0.25. The tephri-phonolite group is ultrapotassic, while basalt-trachy basalt group is shoshonitic; samples do not plot in the calc-alkaline field. In this diagram, the trachyte-latites are intermediate between shoshonitic and ultrapotassic rocks. The strong alkali metal fractionation and moderately high LOI (1.3–5.3 wt.%) suggest some alkali mobility.

The studied rocks were also classified using the immobile element (Th vs. Co) diagram of Hastie *et al.* (2007) (Figure 5(d)). On this diagram, the data mostly plot in the basaltic andesite-andesite and dacite-rhyolite parts of the calc-alkaline and high-K and shoshonitic fields.

These rocks are fractionated and no candidates for primitive magmas were found. Basalts-trachy basalts (Mg# = 33–51) and tephri-phonolites (Mg# = 33–51) are all quite fractionated. The trachyte-latite group is even more differentiated, with very low Mg# values from 3 to 11 (Table 2). In Harker diagrams (Figure 6) the trachyte-latite group has significantly lower contents of TiO_2, CaO, Al_2O_3, MnO, Fe_2O_3 and MgO whereas basalts-trachy basalts and tephri-phonolites show higher contents of these elements. In addition to tephri-phonolite, there are two mafic subgroups: basalt (lower TiO_2, Na_2O, Fe_2O_3) and trachy basalt (higher TiO_2, Na_2O, Fe_2O_3). Na_2O scatters without appreciable correlation

Table 2. Chemical compositions of the E-Saveh volcanic rocks.

Sample	ES-1	ES-2	ES-3	ES-4	ES-5	ES-6	ES-7	ES-24
Rock type	Trachyte	Trachyte	Trachyte	Trachyte	Trachyte	Trachyte	Trachyte	Trachyte
Location	Qom	Qom	Qom	Qom	Qom	Qom	Qom	Qom
SiO_2 (wt.%)	69.0	68.8	67.1	67.0	71.1	68.2	69.7	64.3
TiO_2	0.34	0.37	0.39	0.35	0.32	0.38	0.34	0.44
Al_2O_3	14.1	14.4	14.9	14.4	13.2	14.2	14.1	12.5
Fe_2O_3	3.38	3.73	4.88	3.74	3.97	4.42	3.94	4.32
MnO	0.09	0.06	0.05	0.09	0.03	0.03	0.04	0.05
MgO	0.13	0.37	0.12	0.18	0.08	0.08	0.08	0.37
CaO	3.36	2.93	2.53	2.76	2.09	0.52	0.39	3.44
Na_2O	3.63	3.49	3.37	2.79	2.7	3.14	2.49	2.29
K_2O	5.17	5.14	5.44	7.70	5.85	6.94	7.75	8.59
P_2O_5	0.10	0.11	0.10	0.09	0.06	0.09	0.09	0.11
LOI	1.60	1.40	1.40	1.00	1.20	2.40	1.80	4.50
Total	100.9	100.8	100.3	100.1	100.6	100.4	100.7	101.0
Sc (ppm)	6.54	7.20	9.64	6.42	5.76	7.30	6.74	14.8
V	37.3	48.0	65.0	35.4	29.3	54.7	39.5	64.9
Cr	31.0	4.4	11.2	13.8	5.9	7.7	12.5	9.5
Co	3.19	4.16	3.46	3.86	3.48	3.41	3.85	5.06
Ni	3.3	3.5	9.8	2.4	4.9	6.7	2.8	3.9
Cu	19.0	14.2	22.6	5.7	9.3	16.3	7.3	41.4
Zn	20.7	20.4	16.8	14.3	12.6	11.8	13.2	18.5
Ga	13.7	13.4	15.5	12.2	11.7	13.8	12.5	13.2
Rb	141	132	146	157	142	166	165	138
Sr	136	117	154	122	87.3	92.1	61.4	74.1
Y	21.3	21.5	21.9	16.8	35.7	20.5	16.8	16.3
Zr	146	170	173	122	97.8	153	128	142
Nb	12.2	11.7	11.5	10.7	10.3	11.6	10.6	8.06
Cs	2.85	1.80	1.95	0.780	2.19	1.76	0.900	0.550
Ba	662	531	618	417	421	607	421	381
Hf	4.57	5.19	5.34	4.00	3.29	4.79	4.07	4.15
Ta	0.9	0.8	0.9	0.8	0.7	0.9	0.7	0.4
Pb	10.8	9.22	10.67	8.96	9.38	8.29	6.92	6.70
Th	12.7	12.7	12.4	11.2	10.4	11.9	11.3	6.9
U	3.2	3.1	3.3	2.3	2.3	2.9	2.4	2.0
La	24.0	23.6	23.5	18.6	18.1	18.2	18.4	13.5
Ce	46.2	49.2	44.9	40.2	36.3	38.1	39.6	26.2
Pr	5.22	5.34	5.07	4.37	4.08	4.38	4.40	3.06
Nd	19.3	20.3	19.3	16.6	15.2	17.1	16.2	12.6
Sm	3.82	4.01	4.09	3.08	3.25	3.56	3.22	2.84
Eu	0.73	0.73	0.80	0.55	0.68	0.57	0.54	0.73
Gd	3.62	3.66	3.66	2.71	4.08	3.47	2.68	2.86
Tb	0.57	0.58	0.62	0.44	0.75	0.56	0.43	0.47
Dy	4.04	3.82	4.02	2.88	5.30	3.75	2.78	2.76
Ho	0.83	0.79	0.84	0.64	1.18	0.77	0.63	0.61
Er	2.41	2.41	2.47	2.01	3.18	2.40	1.89	1.97
Tm	0.37	0.38	0.38	0.31	0.48	0.37	0.31	0.31
Yb	2.55	2.68	2.68	2.10	2.90	2.45	2.29	2.25
Lu	0.40	0.40	0.40	0.34	0.43	0.40	0.36	0.33
Mg#	7.1	16	4.6	8.7	3.8	3.5	3.9	14

Sample	MI-1	MI-2	MI-3	MI-4	MI-5	MI-11	MI-12	MI-13
Rock type	Trachyte	Trachyte	Trachyte	Trachyte	Trachyte	Trachyte	Trachyte	Trachyte
Location	Zaviyeh	Zaviyeh	Zaviyeh	Zaviyeh	Zaviyeh	Zaviyeh	Zaviyeh	Zaviyeh
SiO_2 (wt.%)	65.6	66.5	65.8	65.4	64.5	67.1	67.1	66.5
TiO_2	0.60	0.62	0.66	0.69	0.68	0.66	0.54	0.69
Al_2O_3	14.7	14.1	14.9	15.4	14.5	14.0	14.2	14.8
Fe_2O_3	5.01	5.95	4.64	4.55	4.13	5.01	5.77	4.35
MnO	0.16	0.08	0.09	0.12	0.07	0.17	0.10	0.10
MgO	0.34	0.26	0.32	0.20	0.23	0.19	0.17	0.35
CaO	4.24	3.12	3.87	3.80	4.14	3.07	3.64	3.89
Na_2O	2.95	2.78	2.92	2.96	2.96	2.88	2.82	2.67
K_2O	4.50	4.93	4.54	4.67	5.19	4.92	4.91	4.89
P_2O_5	0.22	0.17	0.19	0.20	0.21	0.20	0.19	0.21
LOI	2.00	2.40	2.60	3.00	3.50	2.20	1.20	2.00
Total	100.3	100.9	100.5	100.9	100.2	100.4	100.6	100.4
Sc (ppm)	12.9	14.1	15.3	15.5	15.1	14.5	14.6	15.6
V	39.5	25.5	35.3	29.4	37.6	32.7	29.5	38.6
Cr	9.4	3.1	4.9	5.1	33.7	9.27	6.21	13.6
Co	4.73	2.08	3.41	2.64	2.06	2.96	2.65	3.52
Ni	7.0	3.4	4.7	4.4	4.5	6.7	4.4	4.1
Cu	23.3	13.0	24.8	24.9	19.1	55.5	57.9	70.4
Zn	75.4	21.5	64.7	68.5	18.6	60.3	61.2	89.4
Ga	15.9	16.3	17.7	17.3	16.9	16.3	16.2	17.1
Rb	129	148	132	134	146	143	142	140
Sr	318	157	209	196	205	211	320	215
Y	27.8	23.6	29.0	28.9	25.9	30.1	29.5	31.5
Zr	238	247	253	254	253	246	242	250
Nb	13.6	13.6	14.0	13.9	13.7	13.6	13.3	14.0
Cs	3.39	8.10	2.67	2.76	3.94	3.58	3.37	2.97
Ba	4997	829	846	873	924	1954	7273	1456
Hf	6.85	7.32	7.15	7.31	7.35	6.89	6.98	7.15
Ta	0.9	0.9	0.8	0.9	0.8	0.8	0.9	0.9
Pb	19.4	13.7	15.8	14.8	14.8	11.1	10.6	13.1
Th	10.3	10.5	10.8	10.7	11.1	10.5	10.2	10.9
U	3.2	2.0	2.5	2.5	2.7	2.8	2.8	3.2
La	25.4	24.8	26.1	26.3	24.3	27.2	26.4	28.5
Ce	50.6	48.7	53.3	53.8	48.9	56.0	53.8	57.4
Pr	6.12	5.69	6.43	6.33	5.97	6.58	6.52	6.89
Nd	24.4	22.6	25.4	25.4	24.5	27.0	26.3	28.1
Sm	5.48	4.97	5.69	5.69	5.34	5.86	5.82	6.13
Eu	0.81	1.14	1.23	1.19	1.13	1.12	0.60	1.26
Gd	5.38	4.72	5.50	5.44	4.95	5.77	5.86	6.00
Tb	0.82	0.78	0.88	0.90	0.83	0.91	0.93	0.93
Dy	5.24	4.80	5.97	5.57	5.09	5.85	5.73	5.87
Ho	1.11	1.00	1.15	1.18	1.03	1.17	1.20	1.21
Er	3.28	2.82	3.65	3.57	3.21	3.33	3.46	3.70
Tm	0.52	0.44	0.54	0.52	0.47	0.52	0.51	0.51
Yb	3.40	2.95	3.66	3.56	3.31	3.30	3.36	3.36
Lu	0.50	0.42	0.52	0.53	0.49	0.49	0.52	0.54
Mg#	12	8.0	12	8.0	10	7.0	5.5	14

Sample	MI-14	MI-15	MI-16	MI-17	MI-18	ES-19	ES-20	MI-20
Rock type	Trachyte	Trachyte	Trachyte	Trachyte	Trachyte	Latite	Latite	Latite
Location	Zaviyeh	Zaviyeh	Zaviyeh	Zaviyeh	Zaviyeh	Qom	Qom	Qom
SiO_2 (wt.%)	65.1	65.0	66.7	65.1	56.8	57.6	63.5	49.5
TiO_2	0.68	0.77	0.70	0.67	1.29	0.41	0.51	0.98
Al_2O_3	14.3	15.6	15.2	14.4	15.1	15.1	16.9	16.6
Fe_2O_3	5.04	4.38	4.64	3.57	11.78	5.79	4.97	8.01
MnO	0.12	0.10	0.04	0.11	0.10	0.08	0.05	0.15
MgO	0.21	0.37	0.22	0.24	1.53	0.29	0.26	0.57
CaO	4.19	3.64	2.77	4.30	5.13	7.50	2.08	8.71
Na_2O	2.79	3.05	2.94	2.85	3.24	3.50	2.32	0.83
K_2O	4.83	4.80	4.98	4.90	3.20	6.81	8.41	10.28
P_2O_5	0.20	0.23	0.21	0.21	0.52	0.10	0.13	0.65
LOI	3.50	2.10	2.60	4.60	1.40	3.70	1.60	4.30
Total	100.9	100.1	101.0	100.9	100.0	100.8	100.7	100.6
Sc (ppm)	15.8	9.00	9.43	16.7	24.4	13.9	11.7	16.6
V	39.7	35.5	34.4	39.9	172	60.1	55.5	138
Cr	9.48	5.45	24.2	6.37	3.83	6.32	6.39	79.0
Co	4.04	4.92	3.06	3.81	27.2	4.59	4.74	5.21
Ni	6.7	4.3	3.3	3.8	6.9	4.1	5.5	12.1
Cu	76.0	60.9	35.1	65.5	65.4	44.7	33.9	47.2
Zn	91.7	334	50.8	179	109	27.7	16.9	44.0
Ga	17.1	17.7	17.0	18.8	19.0	13.4	12.6	16.8
Rb	143	142	147	155	88.9	120	134	144
Sr	207	173	108	235	299	61.3	41.0	161
Y	32.8	21.8	18.8	32.3	31.4	19.3	17.7	20.0
Zr	244	254	258	275	179	145	157	181
Nb	13.6	11.8	13.7	15.1	10.8	9.18	7.46	24.2
Cs	3.66	3.99	3.85	3.28	1.81	0.770	0.450	0.640
Ba	872	859	790	1230	553	341	369	2310
Hf	7.09	7.37	7.35	7.21	5.04	4.27	4.69	4.36
Ta	0.9	0.7	0.9	0.9	0.6	0.5	0.3	1.3
Pb	13.4	12.3	12.8	13.7	17.9	5.4	5.6	14.1
Th	10.7	9.1	8.4	11.8	6.9	7.3	7.8	3.0
U	2.6	2.6	2.3	2.8	1.9	8.8	2.2	1.1
La	27.4	20.2	23.5	30.5	24.9	20.3	12.9	38.1
Ce	55.9	39.1	44.8	60.6	52.3	40.4	24.9	70.9
Pr	6.67	4.62	5.29	7.28	6.54	4.70	2.93	8.10
Nd	27.1	18.1	20.2	28.9	27.6	18.5	12.0	31.1
Sm	5.94	3.74	4.07	6.38	6.38	4.09	2.79	5.65
Eu	1.13	0.88	0.76	1.36	1.59	1.08	0.70	1.47
Gd	5.98	3.63	3.67	6.25	6.72	3.88	2.86	5.01
Tb	0.97	0.59	0.54	0.97	0.95	0.60	0.47	0.71
Dy	5.75	3.74	3.20	6.16	6.32	3.87	3.12	4.04
Ho	1.26	0.80	0.65	1.27	1.24	0.78	0.67	0.82
Er	3.72	2.34	2.13	3.73	3.65	2.36	2.14	2.21
Tm	0.55	0.34	0.30	0.53	0.52	0.35	0.33	0.33
Yb	3.47	2.44	2.05	3.64	3.59	2.53	2.42	2.11
Lu	0.56	0.37	0.33	0.57	0.55	0.39	0.36	0.32
Mg#	7.6	14	8.6	12	20	9.0	9.4	12

Sample	ES-8	ES-9	ES-10	ES-11	ES-12	ES-13	ES-14	ES-18
Rock type	Trachy basalt	Trachy basalt	Trachy basalt	Trachy basalt	Trachy basalt	Trachy basalt	Trachy basalt	Trachy basalt
Location	Saveh	Saveh	Saveh	Zaviyeh	Saveh	Zaviyeh	Zaviyeh	Qom
SiO_2 (wt.%)	50.5	50.9	50.2	47.1	49.8	49.7	48.9	46.3
TiO_2	0.77	0.86	1.25	1.02	1.26	1.26	1.24	0.80
Al_2O_3	15.4	15.2	17.3	16.9	17.2	17.3	17.1	18.5
Fe_2O_3	11.1	11.46	8.46	9.10	8.17	10.2	9.24	11.0
MnO	0.25	0.35	0.15	0.22	0.18	0.15	0.17	0.16
MgO	5.80	5.83	2.63	2.19	2.30	2.60	3.36	4.72
CaO	8.24	5.56	8.39	12.65	10.4	7.71	9.11	10.6
Na_2O	3.08	4.31	3.88	3.31	4.09	3.95	3.87	2.40
K_2O	3.31	3.20	2.05	3.15	2.18	2.13	2.07	2.91
P_2O_5	0.23	0.24	0.46	0.25	0.46	0.47	0.46	0.15
LOI	1.30	2.90	5.30	4.20	4.00	4.60	4.80	2.90
Total	100.0	100.8	100.0	100.0	100.1	100.0	100.3	100.4
Sc (ppm)	32.2	33.0	16.5	30.1	17.3	18.1	18.3	31.0
V	295	263	157	265	162	166	166	237
Cr	169.4	151.1	2.09	24.8	7.51	3.21	1.93	19.3
Co	29.2	18.6	14.7	14.1	16.2	16.6	15.5	31.1
Ni	61.0	53.7	3.6	8.8	3.2	4.3	3.4	17.4
Cu	324	12.6	17.5	8.33	24.1	18.6	28.4	61.2
Zn	100	108	102	30.3	92.0	117	96.4	102
Ga	18.0	15.6	18.2	18.0	19.2	19.9	19.2	18.4
Rb	33.7	41.1	34.2	53.9	38.1	37.3	35.8	17.9
Sr	358	187	522	239	541	545	547	357
Y	17.9	16.3	24.2	24.8	27.1	25.8	28.0	15.2
Zr	21.3	19.6	152	81.1	166	173	165	40.3
Nb	2.88	3.12	26.0	5.23	27.9	29.0	27.0	2.43
Cs	0.350	0.350	0.880	1.56	1.03	0.790	0.780	0.310
Ba	679	385	469	384	526	540	550	188
Hf	0.980	0.810	3.59	2.44	3.90	3.89	3.84	1.32
Ta	0.2	0.2	1.4	0.3	1.5	1.5	1.3	0.1
Pb	7.0	3.5	18.4	6.5	7.7	24.1	15.0	9.7
Th	1.2	1.3	3.3	2.8	3.6	3.7	3.5	1.3
U	0.4	0.4	0.8	0.9	0.9	0.9	0.9	0.3
La	9.87	9.12	27.2	26.5	30.2	28.7	30.3	7.04
Ce	20.5	18.9	50.3	48.7	55.5	54.0	55.9	15.4
Pr	2.75	2.48	5.86	5.74	6.41	6.27	6.46	2.05
Nd	12.4	11.8	24.1	23.4	25.7	26.2	25.8	9.49
Sm	3.23	2.88	4.80	5.05	5.36	4.79	5.38	2.48
Eu	1.59	0.86	1.63	1.69	1.81	1.65	1.79	0.83
Gd	3.43	3.09	4.79	5.21	5.23	4.94	5.24	2.95
Tb	0.55	0.50	0.72	0.79	0.81	0.75	0.82	0.46
Dy	3.58	3.33	4.74	4.92	5.15	5.04	5.17	3.03
Ho	0.76	0.67	0.97	0.99	1.07	1.06	1.10	0.63
Er	2.02	1.89	2.71	2.65	2.95	2.78	3.07	1.83
Tm	0.28	0.27	0.37	0.35	0.41	0.42	0.41	0.27
Yb	1.73	1.78	2.50	2.46	2.69	2.75	2.74	1.75
Lu	0.25	0.24	0.37	0.35	0.44	0.41	0.44	0.24
Mg#	51	50	38	33	36	34	42	46

Sample	ES-15	ES-16	ES-17	ES-22	ES-21	ES-23	MI-6	MI-7
Rock type	Basalt	Basalt	Basalt	Basalt	Tephriphonolite	Tephriphonolite	Tephriphonolite	Tephriphonolite
Location	Zaviyeh	Zaviyeh	Zaviyeh	Qom	Qom	Qom	Zaviyeh	Zaviyeh
SiO_2 (wt.%)	49.4	47.2	48.0	47.7	47.1	58.1	52.0	56.1
TiO_2	1.75	0.84	0.83	0.81	1.00	0.45	1.03	1.10
Al_2O_3	15.1	19.2	18.5	19.0	17.6	13.0	17.3	16.9
Fe_2O_3	10.8	11.0	10.9	11.0	10.4	5.13	8.35	7.42
MnO	0.25	0.15	0.14	0.15	0.18	0.05	0.17	0.12
MgO	5.57	4.05	4.55	4.48	2.65	0.19	1.63	0.40
CaO	8.90	10.47	10.5	10.47	9.43	7.34	5.10	4.16
Na_2O	2.97	2.43	2.37	2.31	1.87	3.15	0.43	0.76
K_2O	2.21	2.06	2.15	1.93	7.69	9.10	11.92	12.00
P_2O_5	0.22	0.16	0.15	0.16	0.64	0.11	0.72	0.77
LOI	3.40	3.20	2.90	2.60	2.00	4.10	2.10	1.10
Total	100.5	100.7	101.0	100.6	100.5	100.8	100.7	100.8
Sc (ppm)	32.4	31.6	31.7	30.8	17.5	11.1	13.0	11.1
V	297	280	267	271	231	75.8	76.4	63.4
Cr	137	12.2	13.7	20.0	25.0	7.2	3.2	3.6
Co	29.3	31.0	29.8	30.6	9.94	5.50	9.08	7.36
Ni	61.8	16.2	16.1	16.4	20.2	4.7	3.1	3.2
Cu	323	61.6	62.7	58.5	46.9	41.9	5.38	5.79
Zn	101	106	91.8	121	47.7	27.7	49.5	39.8
Ga	17.9	18.9	18.7	18.4	16.4	14.0	18.7	15.0
Rb	33.7	24.0	26.2	18.4	150	137	199	163
Sr	360	380	368	365	374	197	124	100
Y	17.8	16.3	16.35	15.4	19.7	15.0	23.7	20.3
Zr	21.1	49.1	49.4	42.5	135	141	158	138
Nb	2.88	2.91	2.84	2.63	20.0	9.48	32.9	26.7
Cs	0.340	0.290	0.380	0.250	1.60	0.630	1.16	0.84
Ba	671	215	237	191	2278	341	1972	1647
Hf	0.82	1.59	1.62	1.43	3.12	4.09	4.01	3.35
Ta	0.2	0.2	0.2	0.2	1.0	0.6	1.7	1.4
Pb	6.8	12.0	12.2	13.8	13.9	118	11.5	9.7
Th	1.2	1.3	1.5	1.3	2.0	7.3	4.2	3.7
U	0.4	0.3	0.4	0.3	0.7	2.0	1.1	0.9
La	10.2	7.70	7.73	7.21	31.4	16.7	35.0	28.6
Ce	20.5	16.4	16.9	16.0	62.5	36.0	72.3	58.6
Pr	2.72	2.25	2.23	2.14	7.41	3.96	7.92	6.63
Nd	12.5	10.1	10.4	9.55	29.6	15.7	31.4	26.2
Sm	3.14	2.61	2.80	2.58	5.50	3.39	5.92	4.94
Eu	1.62	0.90	0.84	0.89	1.40	0.72	1.51	1.32
Gd	3.43	2.85	2.95	2.84	5.11	3.08	5.26	4.56
Tb	0.54	0.46	0.47	0.46	0.68	0.45	0.75	0.63
Dy	3.44	3.09	3.26	3.08	3.97	2.97	4.49	3.81
Ho	0.76	0.65	0.66	0.64	0.77	0.57	0.89	0.77
Er	1.98	1.89	1.92	1.74	2.07	1.71	2.64	2.16
Tm	0.27	0.27	0.26	0.27	0.31	0.28	0.36	0.31
Yb	1.77	1.68	1.82	1.77	1.86	1.87	2.24	2.04
Lu	0.27	0.28	0.25	0.24	0.27	0.26	0.34	0.30
Mg#	51	42	45	45	34	6.8	28	10

Sample	MI-8	MI-9	MI-10	MI-19	MI-21	MI-22	MI-23	MI-24
Rock type	Tephriphonolite	Tephriphonolite	Tephriphonolite	Tephriphonolite	Tephriphonolite	Tephriphonolite	Tephriphonolite	Tephriphonolite
Location	Zaviyeh	Zaviyeh	Zaviyeh	Zaviyeh	Qom	Qom	Qom	Qom
SiO_2 (wt.%)	51.2	54.1	54.5	57.6	52.3	49.9	50.3	50.3
TiO_2	1.01	1.03	1.00	1.30	1.12	0.98	0.99	0.99
Al_2O_3	17.2	15.4	15.5	15.2	16.5	16.9	16.8	16.2
Fe_2O_3	8.48	7.19	7.15	11.2	9.11	9.22	8.54	8.22
MnO	0.18	0.16	0.21	0.04	0.40	0.35	0.31	0.35
MgO	0.60	0.51	0.44	0.87	4.33	2.79	3.25	2.99
CaO	5.83	7.50	6.83	4.64	3.82	5.74	5.67	6.27
Na_2O	0.47	0.43	0.45	3.29	1.45	0.37	0.71	0.86
K_2O	11.86	12.07	12.23	3.35	9.02	11.19	10.62	10.7
P_2O_5	0.71	0.74	0.70	0.52	0.71	0.67	0.67	0.72
LOI	2.50	1.60	1.90	2.90	1.40	2.40	2.90	3.20
Total	100.0	100.7	101.0	100.9	100.2	100.5	100.8	100.8
Sc (ppm)	18.6	12.6	9.90	24.4	17.3	17.6	16.9	16.8
V	108	86.0	69.2	171	165	156	143	154
Cr	2.9	11.9	2.9	2.6	88.1	81.7	87.9	81.2
Co	10.1	7.66	5.93	14.8	17.3	9.17	30.9	6.13
Ni	4.1	6.4	5.0	3.7	29.0	13.2	48.9	10.0
Cu	13.9	13.3	12.9	110	5.86	22.7	21.6	206
Zn	50.8	38.5	42.0	94.1	540	247	377	226
Ga	22.5	15.8	14.8	18.7	18.2	17.7	20.6	16.9
Rb	245	201	170	99.6	141	161	138	155
Sr	118	132	132	307	299	710	384	719
Y	28.1	28.7	25.8	28.9	21.5	24.5	22.7	22.0
Zr	223	178	167	179	206	203	202	197
Nb	40.6	30.4	27.1	11.0	26.5	26.4	26.0	25.9
Cs	1.77	1.35	1.29	2.85	0.720	0.520	0.400	0.450
Ba	3170	1073	1352	681	4957	6802	7311	7311
Hf	5.31	3.98	3.88	5.13	4.76	4.64	4.71	4.54
Ta	2.2	1.5	1.5	0.7	1.4	1.4	1.4	1.4
Pb	11.1	18.3	16.5	18.9	20.5	23.2	11.9	22.1
Th	5.7	4.6	4.2	7.0	3.1	3.1	3.0	3.0
U	1.3	1.1	0.7	2.0	1.0	1.2	1.2	1.5
La	41.9	33.0	32.0	25.5	41.0	42.5	36.5	41.7
Ce	84.7	63.7	62.0	52.0	77.7	78.3	71.1	77.2
Pr	9.71	7.42	7.15	6.55	8.72	8.76	7.97	8.65
Nd	37.3	28.7	28.1	27.1	32.8	34.0	30.6	32.7
Sm	7.27	5.83	5.51	6.14	6.04	6.36	5.85	5.83
Eu	1.46	1.60	1.38	1.53	1.31	1.10	0.85	1.04
Gd	6.56	5.63	5.42	6.11	5.25	5.47	5.05	5.14
Tb	0.94	0.83	0.80	0.94	0.72	0.81	0.73	0.76
Dy	5.59	5.05	4.53	5.68	4.38	4.63	4.31	4.16
Ho	1.09	1.05	0.92	1.11	0.84	0.93	0.86	0.85
Er	3.04	3.03	2.70	3.28	2.42	2.67	2.40	2.36
Tm	0.42	0.39	0.38	0.44	0.35	0.36	0.33	0.33
Yb	2.66	2.66	2.46	2.99	2.18	2.30	2.32	2.30
Lu	0.42	0.44	0.38	0.49	0.34	0.33	0.34	0.33
Mg#	12	12	11	13	48	37	43	42

Mg#=100Mg(Mg+Fe)

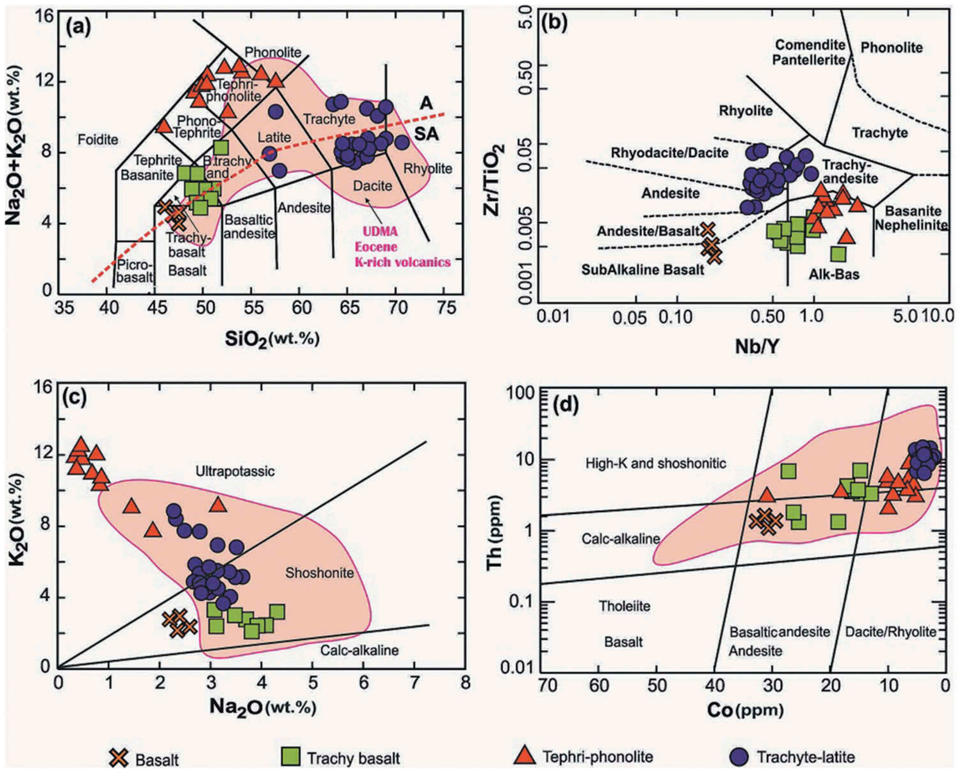

Figure 5. (a) The TAS (total alkali versus silica) diagram of Le Maitre (1989) used to classify the studied rocks and to determine magma series. (b) Nb/Y versus Zr/TiO2 classification based on immobile elements (Winchester and Floyd 1977). (c) Plot of K2O versus Na2O, most of the samples lie within the ultrapotassic and shoshonitic fields. (d) The classification diagram of Hastie *et al*. (2007) based on less mobile elements as Th and Co. Eocene K-rich volcanics geochemical data along UDMA belt from Tutti *et al*. (2008), Ahmadian *et al*. (2009, 2010), Torabi (2009), Etemadi *et al*. (2012) and Yazdani *et al*. (2018).

with SiO_2 (Figure 6). The behaviour of trace elements versus SiO_2 differs from that of the major elements (Figure 7). In the Zr versus SiO_2 diagram (Figure 7), the tephri-phonolite and trachyte-latite groups display sub-horizontal trends, although some trachytes-latites have higher Zr contents. Trachy basalts show lower scattered contents of Zr, but there is an overall increase with SiO_2 (Figure 7) and higher content of these elements for tephri-phonolites. Abundances of La and Nb with silica scatter more than do Sr, Y, Eu, and Yb (Figure 7).

The chondrite-normalized REE patterns of the basalts and trachy basalts (Sun and McDonough 1989) show the two subgroups. Both basalt and trachy basalt are LREE-enriched (Figure 7(a,b)) and positive Eu anomaly is observed in some basaltic rocks. Higher REE contents are observed in trachy basalt compared to basalts. In the primitive mantle normalized diagram (Sun and McDonough 1989), the trachy basaltic group has high LREE. In the primitive mantle normalized diagram, strong depletions of Nb and Ta are observed in basaltic and trachy basaltic rocks and only three trachy basalt samples are not depleted in these elements (Figure 8(e,f)). Trachyte-latites and tephri-phonolites show strongly fractionated REE patterns (Figure 8(c,d)), enriched in LREEs relative to HREEs. LREEs content increases from trachyte-latite to tephri-phonolite. In the primitive mantle normalized diagrams (Sun and McDonough 1989) (Figure 8(g,h)), the trachyte-latite and tephri-phonolite rocks are enriched in large-ion lithophile elements (Pb, K_2O, Ba, and Cs) and moderate depletion in some high field strength elements (TiO_2, Nb, Ta, and Zr).

6.2. Sr-Nd isotope ratios

The $^{87}Sr/^{86}Sr$ (48 samples) and $^{143}Nd/^{144}Nd$ (42 samples) ratios of the Eastern Saveh volcanics are listed in Table 3. The initial $^{76}Sr/^{86}Sr$ and $^{143}Nd/^{144}Nd$ ratios were calculated based on an age of 37 Ma (Verdel *et al*. 2011). Initial $^{87}Sr/^{86}Sr_{(37\ Ma)}$ ranges from 0.7046 to 0.7052 for basalt-trachy basalt, 0.7052–0.7067 for trachyte-latite and 0.7053–0.7074 for tephri-phonolite. These rocks show minor increases in initial $^{87}Sr/^{86}Sr_{(37\ Ma)}$ from basaltic to tephri-phonolitic rocks, consistent with increased continental crust assimilation for high K-rocks. Their $\varepsilon_{Nd}(t)$ values show a narrow range between +0.9 and +1.6 for trachyte-latite, +1.3 to +2.3 for tephri-phonolite and +1.6 to +3.3 for basalt-trachy basalt, suggesting that a homogeneous juvenile mantle source and its melts dominated Eastern Saveh volcanics.

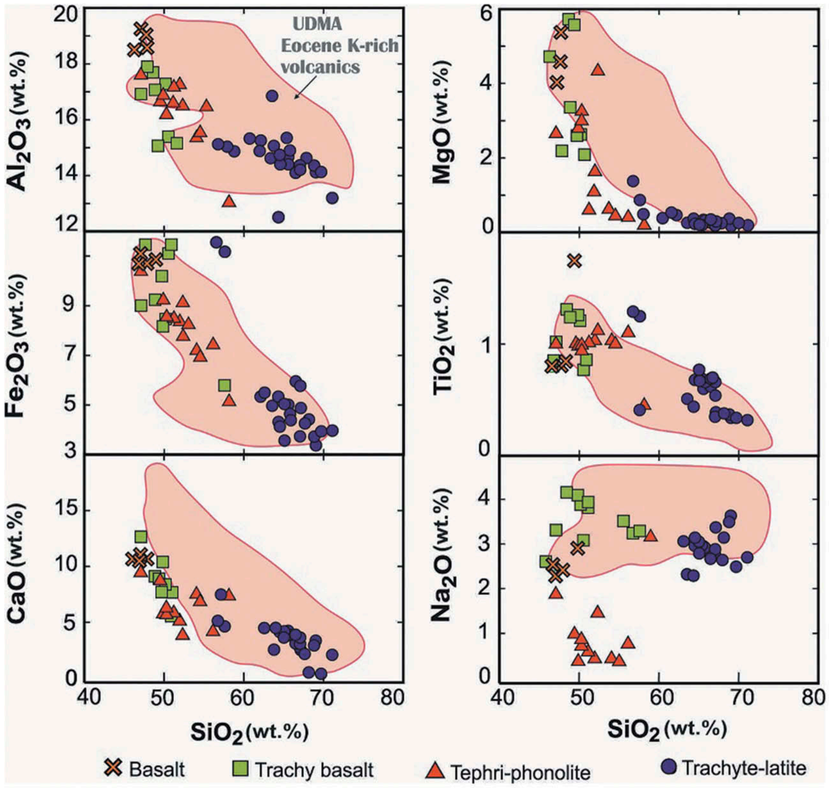

Figure 6. Harker diagrams for major elements showing geochemical relationships for the three groups of eastern Saveh volcanic rocks.

Tephri-phonolitic rocks show higher ratios of $^{87}Sr/^{86}Sr_{(37\ Ma)}$ and higher positive values of $\varepsilon_{Nd}(t)$, suggesting a role for both depleted mantle and crust for the evolution of these magmas. The volcanic rocks plot between the depleted mantle (DM) and enriched mantle (EMII; Zindler and Hart 1986), in the $^{87}Sr/^{86}Sr(i)$-$^{143}Nd/^{144}Nd(i)$ diagram (Figure 9) and trend towards the field of seawater alteration. The alteration intensity increase from basalt-trachy basalt to trachyte-latite and tephri-phonolite groups, respectively.

Eastern Saveh volcanics have lower $^{87}Sr/^{86}Sr$ and higher $^{143}Nd/^{144}Nd$ compared to Miocene ultrapotassic and potassic rocks from Mediterranean ($^{87}Sr/^{86}Sr$ = 0.703–0.709, $^{143}Nd/^{144}Nd$ = 0.5123–0.5128) (Kirchenbaur *et al.* 2012) and Lahrud (NW Iran) potassic rocks ($^{87}Sr/^{86}Sr$ = 0.704–0.705, $^{143}Nd/^{144}Nd$ = 0.5126–0.5127) (Moghadam *et al.* 2018). They display similar Sr-Nd isotope ratios with alkaline volcanics from Mediterranean and Eocene potassic volcanics from Lahrud (Kirchenbaur *et al.* 2012; Moghadam *et al.* 2018) (Figure 9).

7. Discussion

Here we use our results to explore the magma source and tectonic regime for eastern Saveh igneous rocks. We also discuss what these rocks can tell us about UDMA magmatic evolution.

7.1. Source magma

The eastern Saveh volcanic complex is composed of late Eocene (40–37 Ma; Verdel *et al.* 2011) basaltic-trachy basaltic, tephri-phonolite, and trachyte-latite groups with mildly alkaline to shoshonitic signatures. The REE and trace element patterns (Figure 8) compared to OIB, EMORB, and NMORB (Sun and McDonough 1989) show interesting differences. Basalts, some trachy basalts, and trachyte-latites show modest LREE enrichment accompanied by depletion in HFSEs such as Nb, Ta, and Ti, which is typical of subduction zone magmatism (Pearce and Stern 2006; Castillo *et al.* 2007; Pearce 2008; Xu *et al.* 2012; Zheng *et al.* 2013). In contrast, some trachy basalts and tephri-phonolites show more LREE enrichment and less depletion in HFSE and Nb and Ta anomalies. It seems that there are two different mantle sources, one that generated more arc-like magmas (basalts, trachyte-latites, and some trachy basalts) and another that generated more intraplate-like magmas (tephri-phonolites and some trachy basalts). The arc-like source of parental magmas for these suites might reflect partial melting of MORB-OIB asthenospheric mantle that was contaminated by fluids from subducted oceanic crust and sediment-derived melt (Shervais 2001; Pearce and Stern 2006; Dilek *et al.* 2008; Zheng and Hermann 2014; Saccani 2015; Wang *et al.* 2016;

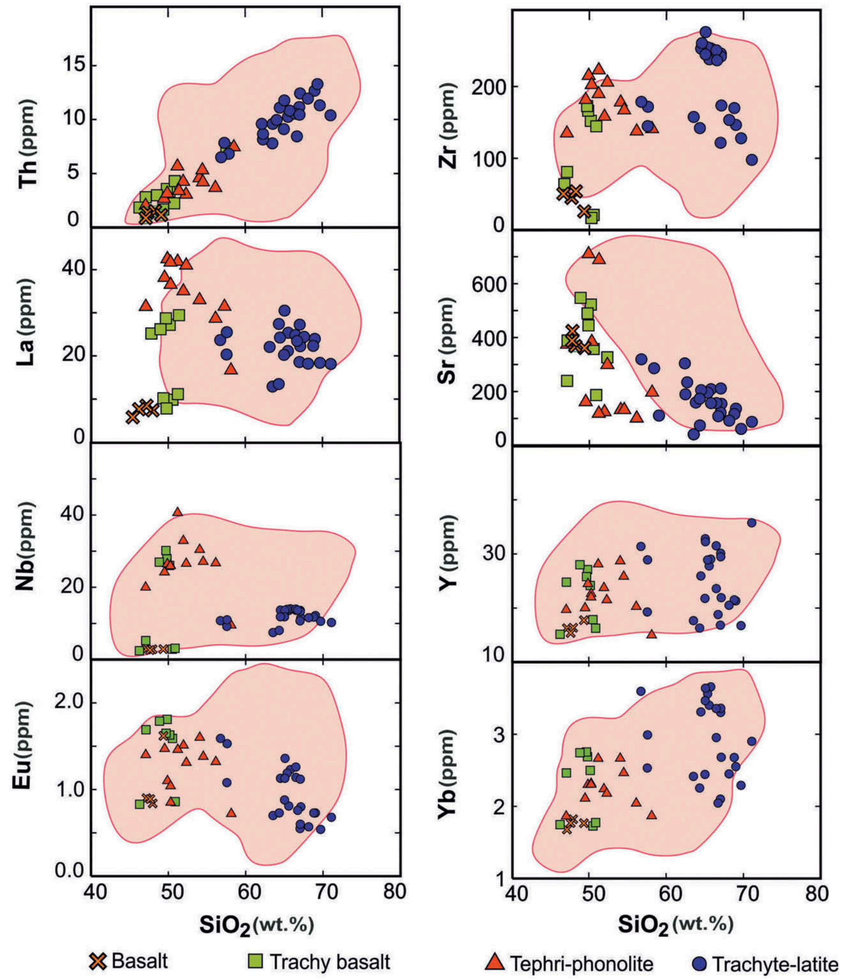

Figure 7. Harker diagrams fir trace elements showing geochemical relationships for the three groups of eastern Saveh volcanic rocks.

Moghadam *et al.* 2018; Xia *et al.* 2018) or by assimilation of continental crust by mantle-derived mafic magmas (Pearce 2008). Both possibilities are consistent with Nb/Yb and Th/Yb ratios in Figure 10(a) where basalts and some trachy basalt plot above the MORB-OIB array (Gorton and Schandl 2000; Pearce 2008; Jian *et al.* 2009; Buchs *et al.* 2013; Gao *et al.* 2018; Liu *et al.* 2019). It is less clear what was the origin of the within-plate like tephri-phonolites and some trachy basalts. One possibility is that these are derived from partial melting of the subcontinental lithospheric mantle as a result of extension and decompression melting.

Radiogenic isotopes do not separate the two mantle sources as well as the trace elements. The studied rocks have $^{87}Sr/^{86}Sr(i)$ of 0.7046–0.7074 and εNd(t) ranging from +0.9 to +3.3, suggesting an OIB-like and slightly depleted mantle source, possibly affected by seawater alteration. In the $^{87}Sr/^{86}Sr(i)$-$^{143}Nd/^{144}Nd(i)$ diagram (Figure 9), island arc and OIB commonly plot between the depleted mantle (DM) and Chondrite Uniform Reservoir (CHUR), consistent with involvement of lithospheric mantle and continental crust (Campbell and Griffiths 1990; Ellam and Cox 1991; Qiu *et al.* 2011). The basalt-trachy basalt, tephri-phonolite and trachyte-latite samples display Sr-Nd isotopic signatures (Figure 9) similar to those of late Eocene Lahrud potassium rocks and Mediterranean ultrapotassic rocks (Kirchenbaur *et al.* 2012; Moghadam *et al.* 2018). These results suggest a broadly similar mantle source for all groups that were variably metasomatized by fluids or sediment melts from subducted seafloor. Eocene arc-like magmas in the Saveh area represented by the studied rocks might reflect addition of Th and other large-ion lithophile elements (LILEs) from subducted sediments or due to interaction with continental crust by assimilation and fractional crystallization (AFC) processes (Verdel *et al.* 2011; Delavari *et al.* 2017; Nouri *et al.* 2018; Yazdani *et al.* 2018; Kazemi *et al.* 2019). Arguments against magmatic control due to continental crustal assimilation include the presence of ultrapotassic intermediate rocks (Figure 5(c)). LILE and LREE enrichment of Eocene magmas are more likely due to metasomatic of mantle

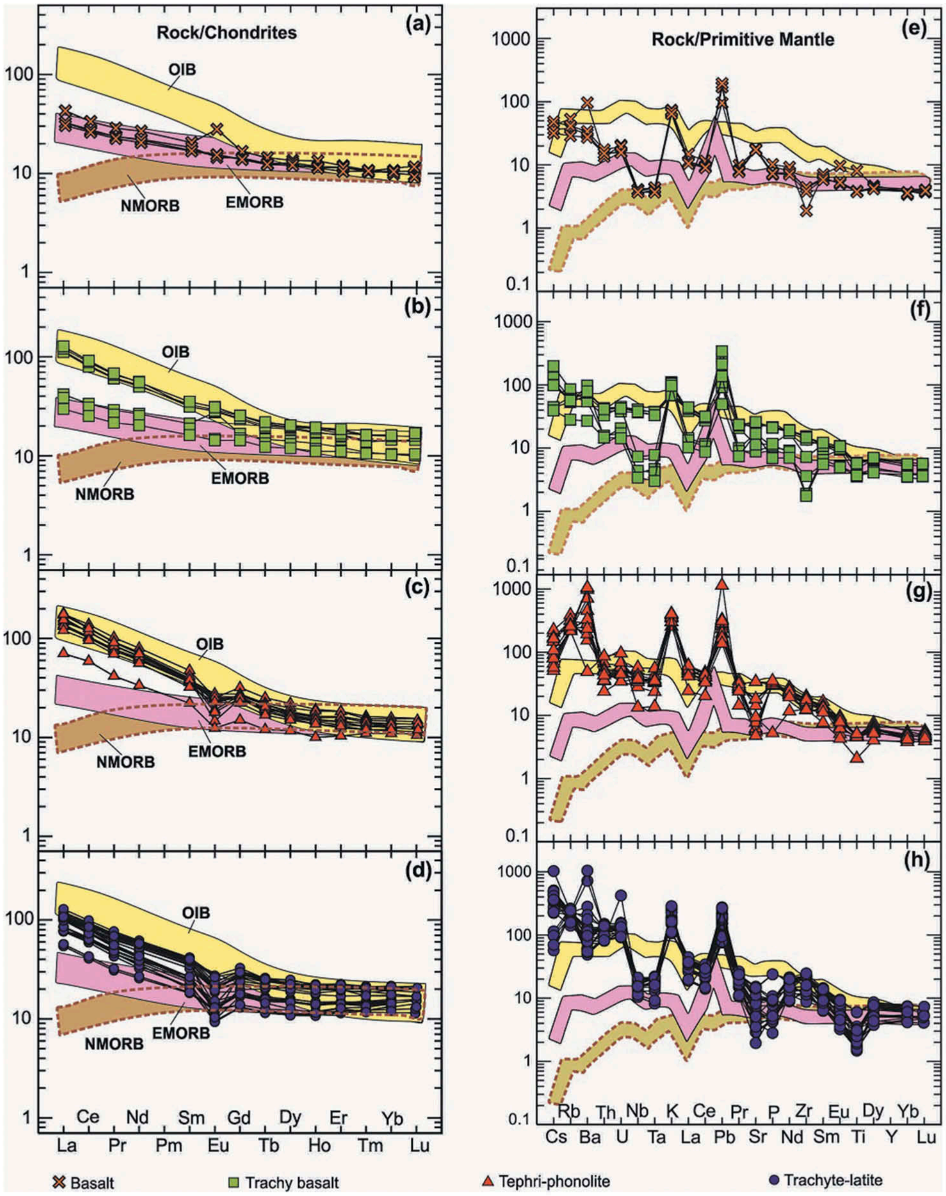

Figure 8. REE and trace element patterns for (a-h) basalt-trachy basalt, tephri-phonolite, trachyte-latite. (a-d) Chondrite-normalized rare earth element (REE) patterns for eastern Saveh volcanic rocks. All show LREE enrichment and nearly at HREE patterns. Note in (a) the two subgroups of basalts (less enriched in LREE) and trachy basalts (more enriched in LREE). (e-h) Trace element concentrations normalized to primitive mantle composition (Sun and McDonough 1989). Note in (e, f) the two subgroups of basalts (deep anomalies in Ta, Nb) and trachy basalts (no anomalies in Ta, Nb). Fields for OIB, EMORB, and NMORB from Sun and McDonough (1989).

source by fluids or melts, including from a subducted slab (Verdel *et al.* 2011; Delavari *et al.* 2017; Nouri *et al.* 2018; Yazdani *et al.* 2018; Kazemi *et al.* 2019).

Further evidence for a mixed arc-like and OIB-like mantle source for eastern Saveh Eocene magmas is gained from examining the Nb/Yb versus Th/Yb plot (Figure 10(a)). The tephri-phonolite and some trachy basalt rocks show the typical within-plate (OIB-like) signature, similar to East African rift and Yellowstone hotspot igneous rocks (GEOROC database); Only the basalt subgroup and some trachy basalt plot in the continental arc field (Figure 10(a)). Additional insights into the mantle sources can be inferred from the La/Nb versus Ba/Nb system (Figure 10(b)). Both magma sources had elevated Ba/Nb, although they can be distinguished on the basis of La/Nb (Wilson and Patterson 2001). The Zr/Y versus Zr systematics of the studied volcanics suggests a within plate tectonic setting for the tephri-

Table 3. Rb-Sr and Sm-Nd abundance and isotopic ratios.

Sample	Rock type	Location	$^{87}Rb/^{86}Sr$	$^{87}Sr/^{86}Sr_{(p)}$	±1SE	$^{87}Sr/^{86}Sr_{(i)}$	$^{147}Sm/^{144}Nd$	$^{143}Nd/^{144}Nd_{(p)}$	±1SE	$^{143}Nd/^{144}Nd_{(i)}$	εNd(t)	T(DM1) (Ga)
ES-1	Trachyte	Qom	3.00	0.706706	0.000006	0.70543	0.120	0.512692	0.000004	0.51267	1.4	0.71
ES-2	Trachyte	Qom	3.27	0.706886	0.000006	0.70549						
ES-3	Trachyte	Qom	2.74	0.706464	0.000007	0.70530	0.128	0.512691	0.000005	0.51267	1.3	0.77
ES-4	Trachyte	Qom	3.73	0.707996	0.000006	0.70641	0.112	0.512691	0.000005	0.51267	1.4	0.66
ES-5	Trachyte	Qom	4.69	0.707494	0.000006	0.70550						
ES-6	Trachyte	Qom	5.21	0.707577	0.000008	0.70536	0.126	0.512700	0.000005	0.51268	1.5	0.74
ES-7	Trachyte	Qom	7.80	0.709050	0.000006	0.70573	0.120	0.512790	0.000004	0.51276	3.3	0.56
ES-24	Trachyte	Qom	5.39	0.708980	0.000006	0.70669	0.137	0.512703	0.000005	0.51268	1.5	0.83
MI-1	Trachyte	Zaviyeh	1.17	0.706383	0.000006	0.70597	0.136	0.512697	0.000005	0.51268	1.3	0.83
MI-2	Trachyte	Zaviyeh	2.73	0.706560	0.000006	0.70559	0.133	0.512688	0.000004	0.51267	1.2	0.82
MI-3	Trachyte	Zaviyeh	1.83	0.706203	0.000007	0.70555	0.135	0.512687	0.000005	0.51267	1.2	0.84
MI-4	Trachyte	Zaviyeh	1.98	0.706226	0.000006	0.70553	0.136	0.512695	0.000004	0.51267	1.3	0.84
MI-5	Trachyte	Zaviyeh	2.06	0.706556	0.000007	0.70582	0.132	0.512697	0.000004	0.51268	1.4	0.80
MI-11	Trachyte	Zaviyeh	1.96	0.706317	0.000007	0.70562	0.132	0.512671	0.000005	0.51265	0.85	0.81
MI-12	Trachyte	Zaviyeh	1.29	0.706133	0.000006	0.70568	0.134	0.512698	0.000004	0.51268	1.4	0.81
MI-13	Trachyte	Zaviyeh	1.88	0.706289	0.000007	0.70562						
MI-14	Trachyte	Zaviyeh	2.01	0.706168	0.000006	0.70546	0.133	0.512707	0.000005	0.51269	1.6	0.79
MI-15	Trachyte	Zaviyeh	2.36	0.706296	0.000006	0.70546	0.125	0.512693	0.000004	0.51267	1.3	0.74
MI-16	Trachyte	Zaviyeh	3.93	0.706368	0.000007	0.70497	0.122	0.512677	0.000005	0.51266	1.0	0.75
MI-17	Trachyte	Zaviyeh	1.91	0.706288	0.000006	0.70561	0.133	0.512685	0.000004	0.51266	1.1	0.83
MI-18	Trachyte	Zaviyeh	0.861	0.705501	0.000005	0.70520	0.140	0.512694	0.000005	0.51267	1.3	0.88
ES-19	Latite	Qom	5.66	0.708490	0.000006	0.70608	0.134	0.512696	0.000004	0.51267	1.4	0.82
ES-20	Latite	Qom	9.50	0.709767	0.000007	0.70572	0.140	0.512707	0.000004	0.51268	1.6	0.86
MI-20	Latite	Qom	2.59	0.706743	0.000006	0.70582	0.110	0.512713	0.000004	0.51270	1.7	0.61
ES-8	Trachybasalt	Saveh	0.273	0.705069	0.000006	0.70495						
ES-9	Trachybasalt	Saveh	0.638	0.705483	0.000007	0.70521	0.147	0.512783	0.000005	0.51275	3.0	0.78
ES-10	Trachybasalt	Saveh	0.190	0.704634	0.000007	0.70455	0.120	0.512781	0.000005	0.51276	3.1	0.57
ES-11	Trachybasalt	Zaviyeh	0.652	0.705434	0.000005	0.70516	0.131	0.512699	0.000005	0.51267	1.4	0.78
ES-12	Trachybasalt	Saveh	0.204	0.704676	0.000007	0.70459	0.126	0.512780	0.000005	0.51276	3.0	0.61
ES-13	Trachybasalt	Zaviyeh	0.198	0.704642	0.000006	0.70456						
ES-14	Trachybasalt	Zaviyeh	0.189	0.704637	0.000007	0.70456	0.126	0.512715	0.000004	0.51269	1.8	0.72
ES-18	Trachybasalt	Qom	0.145	0.704976	0.000006	0.70491	0.158	0.512711	0.000004	0.51277	1.6	1.10
ES-15	Basalt	Zaviyeh	0.271	0.705048	0.000007	0.70493	0.152	0.512798	0.000004	0.51277	3.3	0.80
ES-16	Basalt	Zaviyeh	0.183	0.705016	0.000006	0.70494						
ES-17	Basalt	Zaviyeh	0.206	0.705070	0.000008	0.70498	0.164	0.512720	0.000004	0.51269	1.7	1.19
ES-22	Basalt	Qom	0.146	0.704975	0.000006	0.70491	0.163	0.512714	0.000004	0.51268	1.6	1.19
ES-21	Tephriphonolite	Qom	1.16	0.705838	0.000006	0.70535	0.112	0.512704	0.000004	0.51268	1.6	0.64
ES-23	Tephriphonolite	Qom	2.02	0.708295	0.000006	0.70743	0.131	0.512691	0.000004	0.51267	1.3	0.80
MI-6	Tephriphonolite	Zaviyeh	4.64	0.707256	0.000007	0.70561						
MI-7	Tephriphonolite	Zaviyeh	4.69	0.707290	0.000006	0.70563						
MI-8	Tephriphonolite	Zaviyeh	5.99	0.707917	0.000007	0.70579	0.118	0.512741	0.000004	0.51272	2.3	0.62
MI-9	Tephriphonolite	Zaviyeh	4.43	0.707924	0.000007	0.70635	0.123	0.512722	0.000004	0.51270	1.9	0.68
MI-10	Tephriphonolite	Zaviyeh	3.74	0.707032	0.000006	0.70570	0.119	0.512735	0.000004	0.51272	2.1	0.64
MI-19	Tephriphonolite	Zaviyeh	0.940	0.705578	0.000006	0.70524	0.137	0.512694	0.000004	0.51267	1.3	0.85
MI-21	Tephriphonolite	Qom	1.37	0.706325	0.000006	0.70584	0.111	0.512707	0.000004	0.51269	1.6	0.63
MI-22	Tephriphonolite	Qom	0.658	0.706086	0.000006	0.70585	0.113	0.512710	0.000004	0.51269	1.7	0.64
MI-23	Tephriphonolite	Qom	1.04	0.706238	0.000006	0.70587	0.115	0.512717	0.000004	0.51270	1.8	0.64
MI-24	Tephriphonolite	Qom	0.625	0.706083	0.000007	0.70586	0.108	0.512706	0.000004	0.51269	1.6	0.61

The natural Nd and Sr isotope ratios were normalized based on $^{146}Nd/^{144}Nd = 0.7219$ and $^{86}Sr/^{88}Sr = 0.1194$. Averages and 1σ for isotope ratio standards, JNdi-1 and NBS987, were $^{143}Nd/^{144}Nd = 0.512112 \pm 0.000001$ (n = 2) and $^{87}Sr/^{86}Sr = 0.710263 \pm 0.000010$ (n = 4). The CHUR (Chondritic Uniform Reservoir) values, $^{147}Sm/^{144}Nd = 0.1967$ and $^{143}Nd/^{144}Nd = 0.512638$, were used to calculate the ε^0(DePaolo and Wasserburg 1976). $f_{(Sm/Nd)} = [(^{147}Sm/^{144}Nd)_{sample}/(^{147}Sm/^{144}Nd)_{CHUR}]-1$ and $f_{(Rb/Sr)} = [(^{87}Rb/^{86}Sr)_{sample}/(^{87}Rb/^{86}Sr)_{CHUR}]-1$. $T_{DM1} = 1/\lambda \ln[(^{143}Nd/^{144}Nd)_{sample}-0.512638]/[^{147}Sm/^{144}Nd]_{sample}-0.2137]+1$ (Jahn *et al.* 1999).

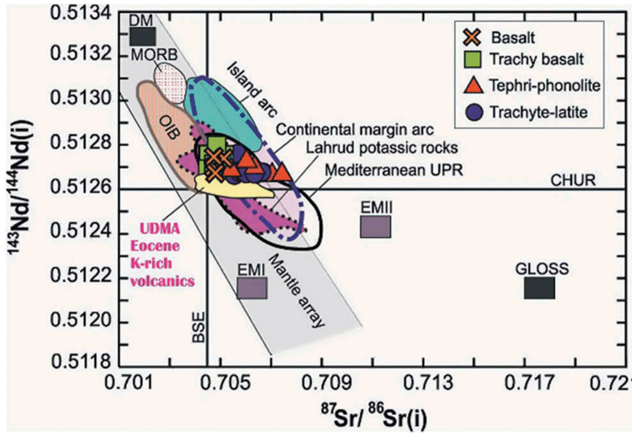

Figure 9. 143Nd/144Nd versus 87Sr/86Sr diagram for eastern Saveh magmatic rocks compared with mantle components HIMU, EM2, and DM. Present day Bulk Earth and CHUR (Chondritic Uniform Reservoir) are also shown. Data for Mediterranean ultrapotassic rocks are from Kirchenbaur *et al.* (2012) and Lahrud potassic rocks from Moghadam *et al.* (2018). Fields for island arc, OIB, and continental margin arc from Eyüboğlu (2010). GLOSS, global subducting sediments (Plank and Langmuir 1998). UDMA Eocene K-rich volcanics (Kahrizak Mountains) from Yazdani *et al.* (2018).

phonolites and some trachy basalts, and a more arc-like signature is seen for basaltic samples (Figure 10(c); Pearce and Norry 1979). For the felsic trachyte-latite group, the Y+ Nb vs. Rb behaviour (Figure 10(d); Pearce *et al.* 1984) indicates a volcanic arc setting, similar to other UDMA felsic lavas.

To investigate the source composition of eastern Saveh basalt-trachy basalt and tephri-phonolites, the Ba/Rb ratio versus Rb/Sr ratio (Duggen *et al.* 2005) was used to examine whether amphibole or phlogopite in the mantle was the source of LILE enrichment. The melts in equilibrium with phlogopite have higher Rb/Sr and lower Ba/Rb ratios than melts derived from amphibole bearing sources (Figure 11(a); LaTourrette *et al.* 1995; Furman and Graham 1999). The basalt-trachy basalt group has the signature of amphibole as the hydrous phase in the source, whereas the presence of sometimes phlogopite and sometimes amphibole is inferred for the source of tephri-phonolite group magmas. The plot of Y versus Dy/Yb ratios (Figure 11(b)) indicates that these melts result from partial melting of a spinel peridotite, consistent with a SCLM lithospheric source. Partial melting of SCLM may have been caused by decompression accompanying upper plate extension.

7.2. *Differentiation and assimilation*

Na_2O vs. K_2O variations (Figure 5(b)) require more complicated processes than just fractional crystallization to cause observed variations within and between groups. Still, fractional crystallization can explain much of the variation. For example, the decrease in MgO, Fe_2O_3 and Co with increasing SiO_2 seen in the Harker diagrams (Figures 6 and 7) reflects mafic mineral (olivine, pyroxene) fractionation from basalt-trachy basalt and tephri-phonolite to trachyte-latite. Correlations between SiO_2 and CaO, Sr, and Na_2O in the three groups suggest K-feldspar and plagioclase fractionation. The MgO and CaO contents decrease with increasing SiO_2, suggesting that fractionation of clinopyroxene was important (Figure 6). Also, negative trends of Fe_2O_3 and TiO_2 with SiO_2 are likely related to fractionation of Fe-Ti oxides. Sr is compatible in plagioclase (Bindeman and Davis 2000; Bedard 2006; Wilson 2007; Nielsen *et al.* 2017; Wilson *et al.* 2017), but not clinopyroxene so the Sr versus MgO plot (Figure 12(a)) can help determine the role of these minerals in fractionation. Sr decreases with MgO in trachyte-latite, but increases with MgO in basalt-trachy basalt. Tephri-phonolite magmas first increased in Sr down to about 2 wt.% MgO and then decreased with lower MgO (Figure 12(a)). These relationships suggest that clinopyroxene fractionation played a significant role in decreasing concentrations of MgO, Fe_2O_3 and CaO, whereas magmatic evolution in more felsic rocks such as trachyte-latites and some tephri-phonolites was mainly controlled by plagioclase fractionation. The minor role of plagioclase fractionation in basalt-trachy basalt magmas is confirmed by the lack of Eu anomalies (Figure 8).

A substantial reduction in the Dy/Yb ratio from basalt-trachy basalt to tephri-phonolite and trachyte-latite rocks with silica content >50% (Figure 12(b)) can only be attributed to hornblende fractionation (Davidson *et al.* 2007, 2012). In this diagram basalt-trachy basalts

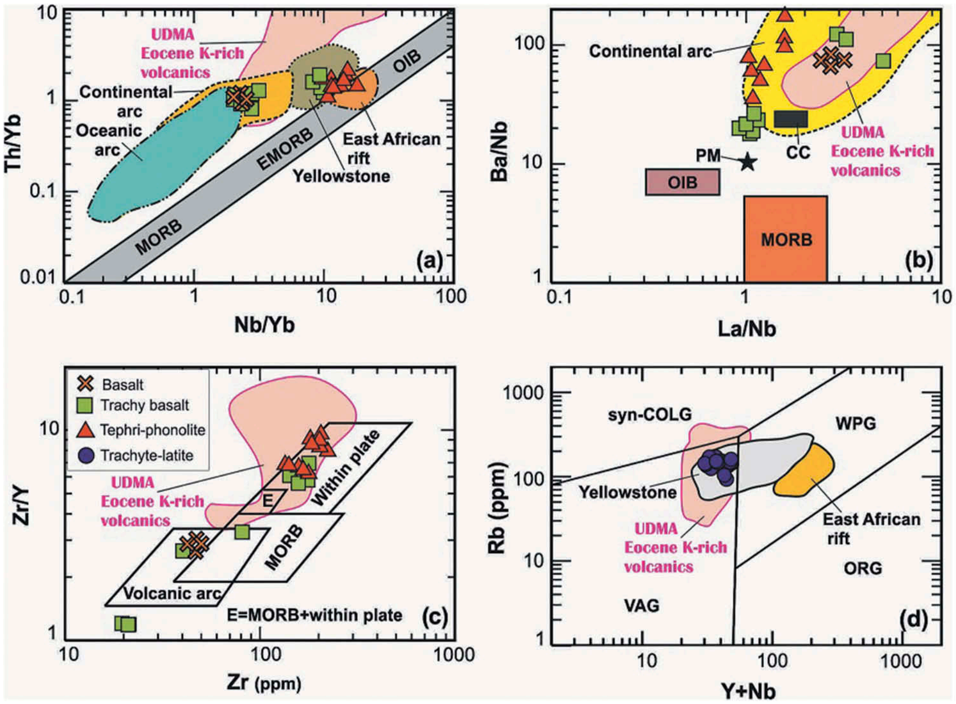

Figure 10. Trace element discriminant plots. (a) Ta/Yb versus Th/Yb diagram (after Pearce 2008) for mafic and intermediate rocks. Note two distinct subgroups: arc-like basalts and OIB-like trachy basalts, which plot close to tephri-phonolites. (b) Ba/Nb versus La/Nb diagram for mafic and intermediate rocks (Zhao *et al.* 2009), which again shows two subgroups of basalt and trachy basalt. Note arc-like behavior of tephri-phonolite. The compositions of different end members are after Wilson and Patterson (2001). Compositions of different components in (a) and (b) are after Wilson and Patterson (2001). (c) The Zr/Y versus Zr systematics of mafic and intermediate rocks shows within-plate affinities of trachy basalt subgroup and tephri-phonolites (Pearce and Norry 1979), although arc-like signature is recognized in basalts. (d) Rb versus Y + Nb diagram (Pearce *et al.* 1984) for trachyte-latites plot in the volcanic arc granite (VAG) field near the within plate granite (WPG), field similar to felsic rocks from the Yellowstone volcanic fields. The data from the East African Rift and Yellowstone from the GEOROC database (http://georoc.mpch-mainz.gwdg.de/georoc/).

and tephri-phonolites show higher Dy/Yb than trachyte-latites. Much variation can be explained by fractionating common minerals such as clinopyroxene, hornblende, and plagioclase in the basalt-trachy basalt, tephri-phonolite and trachyte-latite rocks.

The variation of Nb/Ta and Sm/Nd ratios versus Sr and Nd isotope ratios (Temizel *et al.* 2016) (Figure 13(a,b)) show a nearly horizontal trend with increasing Nb/Ta ratio from trachyte-latite towards basalt-trachy basalt and tephri-phonolite and increasing in Sm/Nd ratio from tephri-phonolite towards trachyte-latite and basalt-trachy basalt. This suggests that the studied volcanic rocks were derived from mantle sources that were isotopically similar. The two subgroups of basalts and trachy basalts are easily distinguished in terms of Nd isotopes but not Sr isotopes.

In order to further evaluate crustal assimilation-crystallization processes, we used Sr-Nd isotope AFC modelling (Figure 13(c)) and different crustal end members such as upper crust, lower crust, and GLOSS (global subducting sediment; Plank and Langmuir (1998)). All basalt-trachy basalt, tephri-phonolite, and trachyte-latite samples display a low ratio of assimilated mass to crystallized mass (r = 0.2), suggesting minor roles of upper crustal contamination and subduction components for magmas represented by the studied rocks.

7.3. Tectonic setting

The UDMA formed as a result of subduction appears as a linear magmatic belt that today exposes ample volcanic sequences and minor intrusive rocks. It is understood as an Andean type magmatic arc formed by subduction of Neo-Tethys oceanic lithosphere beneath Iran (Berberian and Berberian 1981; Verdel *et al.* 2011; Chiu *et al.* 2013). There are several suggested models for the evolution of Palaeogene UDMA magmatism (Berberian and Berberian 1981; Amidi *et al.* 1984; Ghasemi and Talbot 2006; Rezaei-Kahkhaei *et al.* 2011; Verdel *et al.* 2011; Chiu *et al.* 2013; Yazdani *et al.* 2018; Kazemi *et al.* 2019). Verdel *et al.* (2011) recognized three main phases of Palaeogene volcanism in central Iran including: 1) latest Palaeocene-early Eocene phase of pre-extensional arc magmatism; 2) middle Eocene extension with high volcanic output; 3) latest

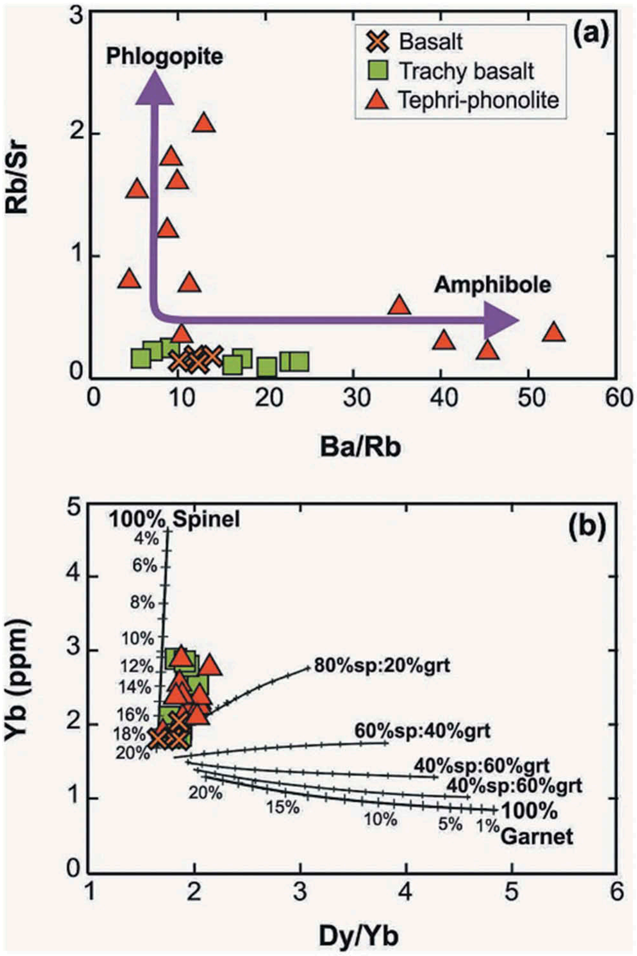

Figure 11. Mineralogical characteristics of eastern Saveh mantle sources. (a) Rb/Sr versus Ba/Rb ratio diagram (Yücel *et al.* 2017) constraints on the nature of LIL-rich hydrous phase. (b) Dy/Yb versus Yb variations for garnet and spinel bearing primitive mantle (PM; McDonough and Frey 1989). Mineral and melt modes for spinel and garnet-lherzolite source are: Ol 0.58(0.10) + Opx 0.27(0.27) + Cpx 0.12(0.50) + Sp 0.03(0.13) (Kinzler 1997) and Ol 0.60(0.05) +Opx 0.21(0.20) +Cpx 0.08(0.30) +Gt 0.12(0.45) (Walter 1998), respectively, in which the members in parentheses indicate the percentage contribution of each mineral to the melt. Tick marks on the melting trajectories represent the percentage of melting for spinel- and garnet-peridotite sources, respectively. Partition coef?cients are from McKenzie and O'Nions (1991).

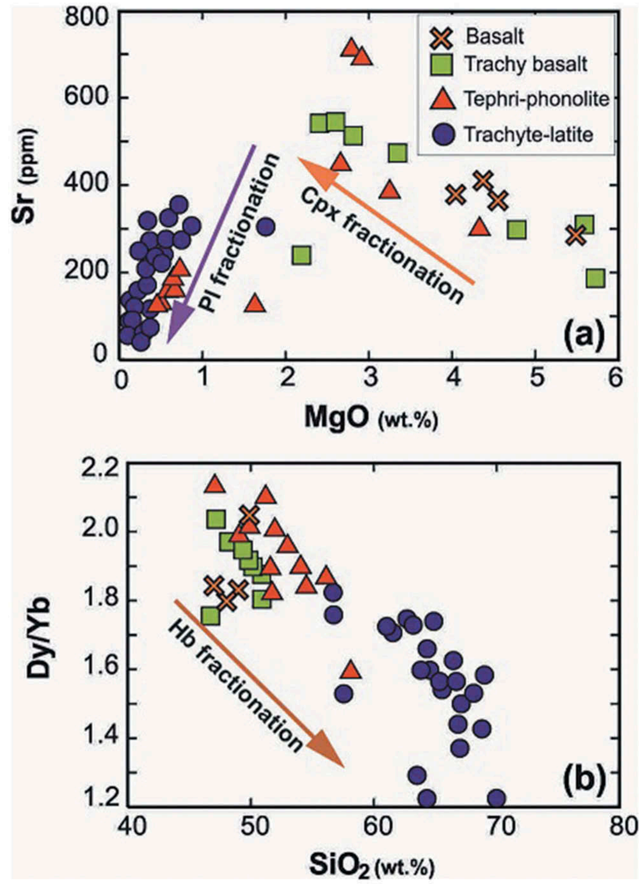

Figure 12. Geochemical variations revealing fractionation of eastern Saveh Eocene magmas. (a) Sr versus MgO diagram showing the importance of clinopyroxene fractionation in mafic and intermediate magmas (>2.5 wt. % MgO) and the importance of plagioclase fractionation in magmas with <2.5 wt. % MgO. (b) Dy/Yb ratio versus silica content, suggesting that hornblende fractionation was important for all three subgroups (Davidson *et al.* 2007).

Eocene-early Oligocene, late to post-extensional volcanism with back arc basin geochemical affinity. Considering the present study and prior data, it appears that Eocene to Oligocene volcanic activity in eastern Saveh was continuous, evolving from calc-alkaline to alkaline (Amidi *et al.* 1984; Ghalamghash 1998; Zamanni and Hossaini 1999). The calc-alkaline association is represented by basalt, whereas tephri-phonolite, trachy basalt, and trachyte-latite represent the alkaline association.

The eastern Saveh volcanics may reflect a rifted arc due to the segmentation of the subducting plate (Ghasemi and Talbot 2006). In late Eocene time, the nature of subduction changed (Ghasemi and Talbot 2006) and the subducting slab experienced strong slab rollback. As a result, eastern Saveh magmatism reflected two processes: 1) normal flux partial melting of asthenosphere to create parental magmas of basalt and some trachy basalts; and 2) parental magmas for tephri-phonolite and other trachy basalts were generated by decompression of SCLM as a consequence of extension due to slab rollback (Figure 14). During this episode, a large volume of volcanic rocks with interbedded limestone and detrital sediments developed (Amidi *et al.* 1984; Ghalamghash 1998; Zamanni and Hossaini 1999; Verdel *et al.* 2011; Chiu *et al.* 2013). The isotopic data largely confirm the involvement of subcontinental lithospheric mantle in the evolution of all the eastern Saveh magmatic rocks. It may be that the more arc-like magmas were derived from near the base

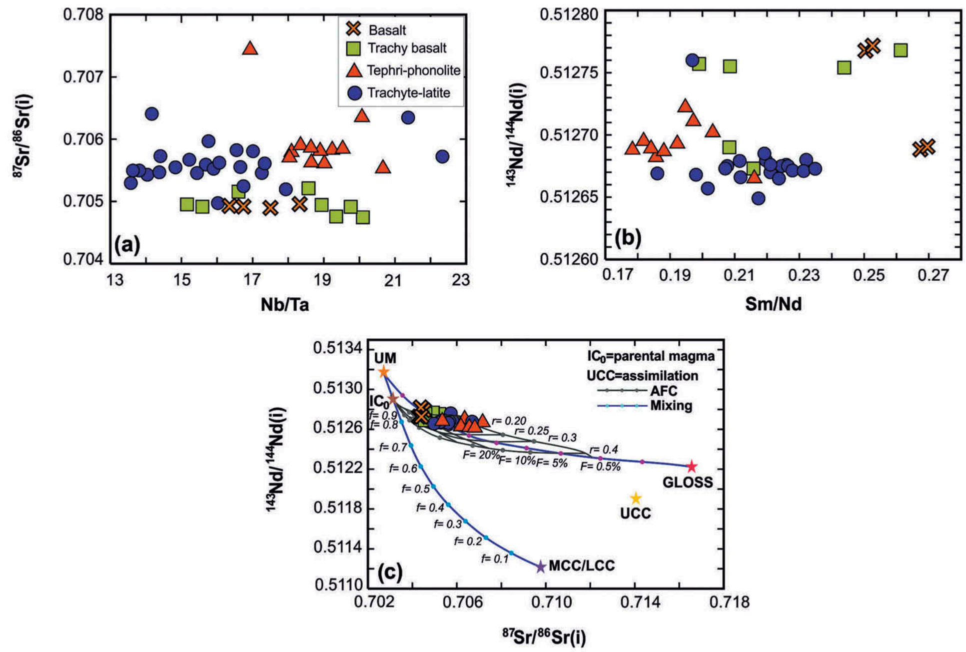

Figure 13. (a) (87Sr/86Sr)i versus Nb/Ta, suggesting that fractionation was more important than assimilation. (b) (143Nd/144Nd)i versus Sm/Nd, which also suggests that fractionation was more important than assimilation and also that basalt and trachy-basalt subgroups can be distinguished on the basis of Nd isotopes. (c) Assimilation-fractional crystallization model (DePaolo 1981) for eastern Saveh igneous rocks. Representative AFC curves using (87Sr/86Sr)i versus (143Nd/144Nd)i are for various combinations of a hypothetical parental magma (IC0; 87/86Sr = 0.70286 and 143Nd/144Nd = 0.512917, Sr = 80 ppm, and Nd = 220 ppm), assimilate (UCC; 87/86Sr = 0.71463 and 143Nd/144Nd = 0.511843, Davies *et al.* (1985); Sr = 26 ppm and Nd = 350 ppm, Taylor and Mclennan (1985) and bulk distribution coef?cients (DSr = 0.85, DNd = 0.10). Tick marks indicate the degree of crystallization (F) and are given in intervals of 0.5 to a maximum of 0.90 (r = 0.1–0.4, for all curves). Theoretical mixing lines of are between upper mantle (UM; 87Sr/86Sr = 0.7025 and 143Nd/144Nd = 0.5132, Rehkamper and Hofmann (1997); Sr = 19 ppm and Nd = 190 ppm, Zindler *et al.* (1984) and middle/lower continental crust (MCC/LCC; 87Sr/86Sr = 0.71014 and 143Nd/144Nd = 0.5111, Ben Othman *et al.* (1984); Sr = 300 ppm and Nd = 24 ppm, Rudnick and Fountain (1995)); GLOSS (Global Subducting Sediments) from Plank and Langmuir (1998). Tick marks indicate the degree of crystallization and are given at intervals of 0.1 to a maximum of 0.90 and f: fraction of component UM in product magma.

of the SCLM where it was exposed to more subduction-related fluids whereas the more rift-like magmas were derived from shallower parts of the SCLM which were less exposed to such fluids. These magmas fractionated extensively but did not mix much. Fractionation led to the development of trachyte-latite magma as a result of low-pressure differentiation of arc-like magmas.

Concluding remarks

The eastern Saveh volcanic complex in the Urumieh-Dokhtar magmatic belt of central Iran contains fractionated arc-like and rift-like magmatic rocks that can be subdivided into three major groups: basalt-trachy basalt, tephri-phonolite, and trachyte-latite. Each of the three groups occurs in the ~ 1.5-km thick Eocene volcanic sequence around Saveh: basalt-trachybasalt is found at top and bottom, trachyte-latite is found in the lower half of the sequence, and tephri-phonolite is found in the middle of the section. All lavas are interbedded with shallow marine sediments, suggesting that rifting accompanied igneous activity.

The volcanic rocks evolved mildly alkaline, high-K to shoshonitic compositions. Two distinct mantle sources are identified, one that generated more arc-like magmas (basalts, trachyte-latites, and some trachy basalts) and another that generated more intraplate-like magmas (tephri-phonolites and some trachy basalts). Variable depletion in Nb and Ta relative to LILEs, moderate LREEs/HREEs, and high Th/Yb ratios, and Sr–Nd isotope data suggest that the subcontinental lithospheric mantle was variably affected by subduction components and that both flux melting and decompression melting were important for UDMA magmagenesis. Fractional crystallization played an important role in magma evolution. Our results indicate that overriding plate extension led to decompression melting of variably metasomatized SCLM to form a mixed suite of OIB-like and arc-like mafic melts that experienced magma mixing and

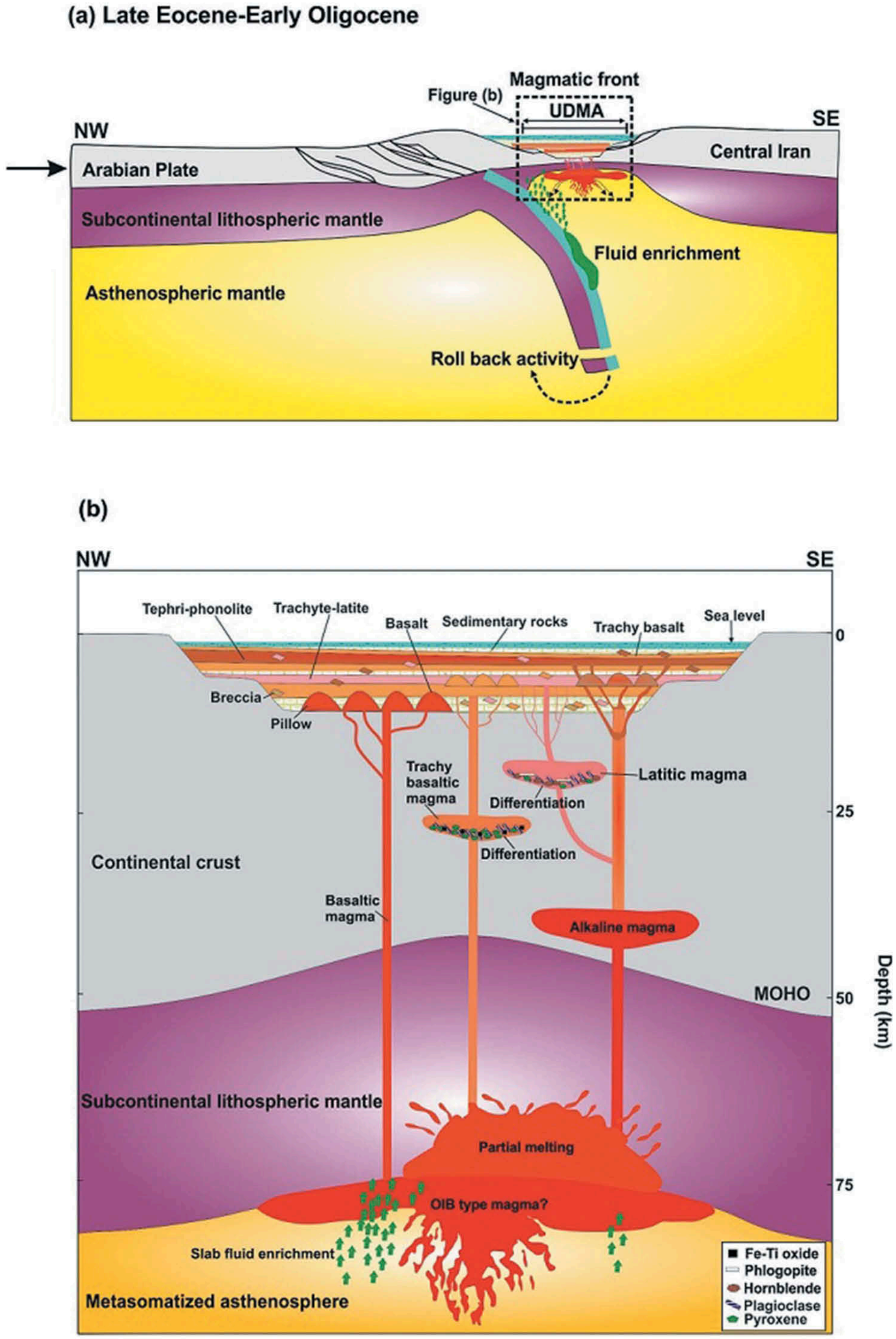

Figure 14. Cartoon showing the preferred petrogenetic evolutionary model for the parental magma(s) generation in an extensional arc due to slab rollback (a). (b) A large volume of volcanic rocks with interbedded limestone and detrital sediments developed (Amidi *et al*. 1984; Ghalamghash 1998; Zamanni and Hossaini 1999; Verdel *et al*. 2011; Chiu *et al*. 2013). During extension, subcontinental lithospheric mantle above the subducted slab was variably metasomatized and upwelled due to increased temperature. Partial melting of subcontinental lithospheric mantle (SCLM) that was less exposed to subduction-related fluids produced the tephri-phonolite and some trachy basalt volcanics. Partial melting of SCLM that was more affected by subduction zone fluids generated basalts and some trachy basalts. The final stage involved the development of trachyte-latite magma, produced from low-pressure differentiation and contamination of more mafic parental melts of enriched mantle over the subduction zone.

extensive assimilation-fractional crystallization to produce the different types of Eocene volcanic rocks in the eastern Saveh area.

Highlights

- Sr-Nd isotope ratios suggest a moderately metasomatized mantle source for these rocks.
- There was minor involvement of continental crust in generating of volcanic magma.
- Partial melting of metasomatized asthenospheric and subcontinental lithosphere was the source of volcanic rocks.
- Extensional regime developed due to the rollback of the subducted Neo-Tethys oceanic plate.

Acknowledgments

This research was supported by University of Kurdistan in Iran and Nagoya University in Japan. Analytical studies were supported by the Japan Society for Promotion of Sciences (JSPS) KAKENHI grant number 17H011671. This is UTD Geosciences contribution number 1331. We are grateful to S. Khodaparast, A. Mehrvarz and F. Rezaei for the help in the field and technical assistance.

Disclosure statement

No potential conflict of interest was reported by the authors.

Funding

This research was supported by University of Kurdistan in Iran and Nagoya University in Japan. Analytical studies were supported by Japan Society for Promotion of Sciences (JSPS) KAKENHI grant number 17H011671. This is UTD Geosciences contribution number 1331.

ORCID

Hossein Azizi http://orcid.org/0000-0001-5686-4340

References

Ahmadian, J., Bahadoran, N., Torabi, G., and Murata, M., 2010, Geochemistry and petrogenesis of volcanic rocks from the arousan-e-kaboudan (NE of Anarak): Petrology, v. 1, p. 103–120.*(in Persian)*

Ahmadian, J., Haschke, M., Mcdonald, I., Regelous, M., Ghorbani, M.R., Emami, M.H., and Murata, M., 2009, High magmatic flux during Alpine-Himalayan collision: constraints from the kal-e-kafi complex, central Iran: Geological Society of America Bulletin, v. 121, p. 857–868. doi: 10.1130/B26279.1

Ahmadzadeh, G., Jahangiri, A., Lentz, D., and Mojtahedi, M., 2010, Petrogenesis of Plio-Quaternary post-collisional ultrapotassic volcanism in NW of Marand, NW Iran: Journal of Asian Earth Sciences, v. 39, no. 1–2. p. 37–50.doi: 10.1016/j.jseaes.2010.02.008

Alavi, M., 1994, Tectonic of the Zagros orogenic belt of Iran: New data an interpretations: Tectonophysics, v. 229, p. 211–238.doi: 10.1016/0040-1951(94)90030-2

Alavi, M., 2004, Regional stratigraphy of the Zagros fold-thrust belt of Iran and its proforeland evolution: American Journal of Science, v. 304, p. 1–20.doi: 10.2475/ajs.304.1.1

Amidi, S.M., Emami, M.H., and Michel, R., 1984, Alkaline character of Eocene volcanism in the middle part of central Iran and its geodynamic situation: Geologische Rundschau, v. 73, p. 917–932.doi: 10.1007/BF01820882

Amidi, S.M., Shahrabi, M., and Navai, I., 2004, Geological Map of Zaviye: Geology Survey of Iran. scale 1:100000, NO. 6160.

Ayati, F., 2015, Geochemistry investigations of volcanic rocks in Salafchegan–Khorhe sheet with emphasize on Sr-Nd isotopic data: Journal of Tethys, v. 3, p. 163–181.

Azizi, H., and Stern, R.J., 2019, Jurassic igneous rocks of the central Sanandaj–Sirjan zone (Iran) mark a propagating continental rift, not a magmatic arc: Terra Nova, v. 31, p. 415–423.doi: 10.1111/ter.12404

Bedard, J.H., 2006, Trace element partitioning in plagioclase feldspar, Geochim: Cosmochim. Acta, v. 70, p. 3717–3742. doi: 10.1016/j.gca.2006.05.003

Ben Othman, D., Polve, M., and Allegre, C.J., 1984, Nd–Sr isotopic composition of granulites and constraints on the evolution of the lower continental crust: Nature, v. 307, p. 510–515.doi: 10.1038/307510a0

Berberian, F., and Berberian, M., 1981, Tectono-plutonic episodes in Iran: Zagros Hindu Kush Himalaya geodynamic evolution, eds., Gupta, H.K., and Delany:, F.M., American Geophysical Union: Vol. 3, 33–69 p. doi: 10.1029/GD003p0005

Berberian, M., and King, G.C.P., 1981, Towards a paleogeography and tectonic evolution of Iran: Canadian Journal of Earth Sciences, v. 18, p. 210–265.doi: 10.1139/e81-019

Bindeman, I.N., and Davis, A.M., 2000, Trace element partitioning between plagioclase and melt: Investigation of dopant influence on partition behavior: Geochimica et cosmochimica acta, v. 64, p. 2863–2878.doi:10.1016/S0016-7037(00)00389-6

Buchs, D.M., Bagheri, S., Martin, L., Hermann, J. and Arculus, R., 2013, Paleozoic to Triassicocean opening and closure preserved in Central Iran: Constraints from the geochemistry of meta-igneous rocks of the Anarak area: Lithos, v. 172, p. 267–287.doi: 10.1016/j.lithos.2013.02.009

Caillat, C., Dehlavi, P. and Jantin, B.M., 1978, Géologie de la région de Saveh (Iran): Contribution à l'étude du volcanisme et du plutonisme tertiaires de la zone de l'Iran central (Doctoral dissertation).

Campbell, I.H., and Griffiths, R.W., 1990, Implications of mantle plume structure for the evolution of flood basalts: Earth and Planetary Science Letters, v. 99, p. 79–93.doi: 10.1016/0012-821X(90)90072-6

Castillo, P.R., Rigby, S.J., and Solidum, R.U., 2007, Origin of high field strength element enrichment in volcanic arcs: Geochemical evidence from the Sulu Arc, southern Philippines: Lithos, v. 97, p. 271–288.doi: 10.1016/j.lithos.2006.12.012

Chiu, H.Y., Chung, S.L., Zarrinkoub, M.H., Mohammadi, S.S., Khatib, M.M., and Iizuka, Y., 2013, Zircon U–Pb age constraints from Iran on the magmatic evolution related to Neotethyan subduction and Zagros orogeny: Lithos, v. 162, p. 70–87.doi: 10.1016/j.lithos.2013.01.006

Conticelli, S., Marchionni, S., Rosa, D., Giordano, G., Boari, E., and Avanzinelli, R., 2009, Shoshonite and sub-alkaline magmas from an ultrapotassic volcano: Sr–Nd–Pb isotope data on the Roccamonfina volcanic rocks, Roman Magmatic Province, Southern Italy: Contributions to Mineralogy and Petrology, v. 157, p. 41–63.doi: 10.1007/s00410-008-0319-8

Dai, S., Nechaev, V.P., Chekryzhov, I.Y., Zhao, L., Vysotskiy, S.V., Graham, I., Ward, C.R., Ignatiev, A.V., Velivetskaya, T.A., Zhao, L., and French, D., 2018, A model for Nb–Zr–REE–Ga enrichment in Lopingian altered alkaline volcanic ashes: Key evidence of H-O isotopes: Lithos, v. 302, p. 359–369.doi: 10.1016/j.lithos.2018.01.005

Davarpanah, A., 2009, Magmatic evolution of the eocene volcanic rocks of the Bijgerd Kuh E Kharchin area, Urumieh-Dokhtar zone, Iran [Master of Science Thesis]: Georgia State University.

Davidson, J., Turner, S., Handley, H., Macpherson, C., and Dosseto, A., 2007, Amphibole "sponge" in arc crust? Geology, v. 35, p. 787–790.doi: 10.1130/G23637A.1

Davidson, J., Turner, S., and Plank, T., 2012, Dy/Dy*: Variations arising from mantle sources and petrogenetic processes: Journal of Petrology, v. 54, no. 3. p. 525–537.doi: 10.1093/petrology/egs076

Davies, G., Gledhill, A., and Hawkesworth, C., 1985, Upper crustal recycling in southern Britain: Evidence from Nd and Sr isotopes: Earth and Planetary Science Letters, v. 75, p. 1–12.doi: 10.1016/0012-821X(85)90045-7

Delavari, M., Rezaei, P., and Dolati, A., 2017, Eocene magmatism of Orumieh-Dokhtar belt (North of Saveh): Variation of volcanic suites in an extensional tectonic setting: Journal of Researches in Earth Sciences, v. 30, p. 1–16.*(in Persian)*

DePaolo, D.J., 1981, Trace element and isotopic effects of combined wallrock and fractional crystallization: Earth and Planetary Science Letters, v. 53, p. 189–202.doi:10.1016/0012-821X(81)90153-9

DePaolo, D.J., and Wasserburg, G.J., 1976, Nd isotopic variations and petrogenetic models: Geophysical Research Letters, v. 3, p. 249–252.doi: 10.1029/GL003i005p00249

Dilek, Y., Furnes, H., and Shallo, M., 2008, Geochemistry of the Jurassic Mirdita Ophiolite (Albania) and the MORB to SSZ evolution of a marginal basin oceanic crust: Lithos, v. 100, p. 174–209.doi: 10.1016/j.lithos.2007.06.026

Duggen, S., Hoernle, K., van den Bogaard, P., and Garbe-Schönberg, D., 2005, Post-collisional transition from subduction-to intraplate-type magmatism in the westernmost Mediterranean: Evidence for continental-edge delamination of subcontinental lithosphere: Journal of Petrology, v. 46, p. 1155–1201.doi: 10.1093/petrology/egi013

Ellam, R.M., and Cox, K.G., 1991, An interpretation of Karoo picrite basalts in terms of interaction between asthenospheric magmas and the mantle lithosphere: Earth and Planetary Science Letters, v. 105, no. 1–3. p. 330–342.doi: 10.1016/0012-821X(91)90141-4

Etemadi, B., Taghipour, B., Ghobadi, A., Eslami, A., and Salimi Darani, M., 2012, Petrography and tectonic setting investigation of Tertiary igneous rocks in the Nodoushan area (SW of Sadough, Yazd province): Petrology, v. 10, p. 13–26.*(in Persian)*

Ewart, A., 1982, The mineralogy and petrology of Tertiary–Recent orogenic volcanic rocks: With special reference to the andesitic–basaltic compositional range, Thorpe, R.S., ed., Andesites: Orogenic Andesites and Related Rocks: John Wiley, New York, 25–98 p.

Eyüboğlu, Y., 2010, Late Cretaceous high-K volcanism in the eastern Pontide orogenic belt: Implications for the geodynamic evolution of NE Turkey: International Geology Review, v. 52, p. 142–186.doi: 10.1080/00206810902757164

Furman, T., and Graham, D., 1999, Erosion of lithospheric mantle beneath the East African Rift system: Geochemical evidence from the Kivu volcanic province: In Developments in Geotectonics, v. 24, p. 237–262.doi: 10.1016/S0419-0254(99)80014-7

Gao, Z., Zhang, H.F., Yang, H., Pan, F.B., Luo, B.J., Guo, L., Xu, W. C., Tao, L., Zhang, L.Q., and Wu, J., 2018, Back-arc basin development: Constraints on geochronology and geochemistry of arc-like and OIB-like basalts in the Central Qilian block (Northwest China): Lithos, v. 310, p. 255–268.doi: 10.1016/j.lithos.2018.04.002

Ghalamghash, J., 1998, Geological Map of Saveh: Geology Survey of Iran, scale 1:100000, NO. 6060.

Ghasemi, A., and Talbot, C.J., 2006, A new tectonic scenario for the Sanandaj–Sirjan Zone (Iran): Journal of Asian Earth Sciences, v. 26, p. 683–693.doi: 10.1016/j.jseaes.2005.01.003

GiGill, R., 2011. Igneous rocks and processes: A practical guide. John wiley & sons. 415 p.

Gorton, M.P., and Schandl, E.S., 2000, From continents to island arcs: A geochemical index of tectonic setting for arc-related and within-plate felsic to intermediate volcanic rocks: The Canadian Mineralogist, v. 38, p. 1065–1073.doi: 10.2113/gscanmin.38.5.1065

Haghighi Bardineh, S.N., Zarei Sahamieh, R., Zamanian, H., and Ahmadi Khalaji, A., 2018, Geochemical, Sr-Nd isotopic investigations and U-Pb zircon chronology of the Takht granodiorite, west Iran: Evidence for post-collisional magmatism in the northern part of the Urumieh-Dokhtar magmatic assemblage: Journal of African Earth Sciences, v. 139, p. 354–366.doi: 10.1016/j.jafrearsci.2017.12.030

Hassanzadeh, J., 1993, Metallogenic and tectonomagmatic events in the SE sector of the Cenozoic active continental margin of central Iran (Shahr e Babak area, Kerman Province) [Ph.D. thesis]: University of California. 204 p

Hastie, A.R., Kerr, A.C., Pearce, J.A., and Mitchell, S.F., 2007, Classification of altered volcanic island arc rocks using immobile trace elements: Development of the Th–Co discrimination diagram: Journal of Petrology, v. 48, p. 2341–2357. doi: 10.1093/petrology/egm062

Hatzfeld, D., and Molnar, P., 2010, Comparisons of the kinematics and deep structures of the Zagros and Himalaya and of the Iranian and Tibetan plateaus and geodynamic implication: Reviews of Geophysics, v. 48, no. RG2005. doi:10.1029/2009RG000304

Huang, D., and Hou, Q., 2017, Devonian alkaline magmatism in the northern North China Craton: Geochemistry, SHRIMP zircon U-Pb geochronology and Sr-Nd-Hf isotopes: Geoscience Frontiers, v. 8, p. 171–181.doi: 10.1016/j.gsf.2016.02.006

Jahangiri, A., 2007, Post-collisional Miocene adakitic volcanism in NW Iran: Geochemical and geodynamic implications: Journal of Asian Earth Sciences, v. 30, no. 3–4. p. 433–447. doi: 10.1016/j.jseaes.2006.11.008

Jahn, B.M., Wu, F., Lo, C.H., and Tsai, C.H., 1999, Crust–mantle interaction induced by deep subduction of the continental crust: Geochemical and Sr–Nd isotopic evidence from post-collisional mafic–ultramafic intrusions of the northern Dabie complex, central China: Chemical Geology, v. 157, p. 119–146.doi: 10.1016/S0009-2541(98)00197-1

Jian, P., Liu, D., Kröner, A., Zhang, Q., Wang, Y., Sun, X., and Zhang, W., 2009, Devonian to Permian plate tectonic cycle of the Paleo-Tethys Orogen in southwest China (I):

Geochemistry of ophiolites, arc/back-arc assemblages and within-plate igneous rocks: Lithos, v. 113, p. 748–766.doi: 10.1016/j.lithos.2009.04.004

Kazemi, K., Kananian, A., Xiao, Y., and Sarjoughian, F., 2019, Petrogenesis of Middle-Eocene granitoids and their mafic microgranular enclaves in central Urmia-Dokhtar Magmatic Arc (Iran): Evidence for interaction between felsic and mafic magmas: Geoscience Frontiers, v. 10, p. 705–723.doi: 10.1016/j.gsf.2018.04.006

Kepezhinskas, N., Kamenov, G.D., Foster, D.A., and Kepezhinskas, P., 2019, Petrology and geochemistry of Alkaline Basalts and Gabbroic xenoliths from Utila Island (Bay Islands, Honduras): Insights into back-Arc processes in the Central American Volcanic Arc:: Lithos, p. 105–306. doi: 10.1016/j.lithos.2019.105306

Kinzler, R.J., 1997, Melting of mantle peridotite at pressure approaching the spinel to garnet transition: Application to mid-ocean ridge basalt petrogenesis: Journal of Geophysical Research: Solid Earth, v. 102, p. 853–874.doi: 10.1029/96JB00988

Kirchenbaur, M., Munker, C., Schuth, S., Garbe-Schonberg, D., and Marchev, P., 2012, Tectonomagmatic constraints on the sources of Eastern Mediterranean K-rich lavas: Journal of Petrology, v. 53, p. 27–65.doi: 10.1093/petrology/egr055

LaTourrette, T., Hervig, R.L., and Holloway, J.R., 1995, Trace element partitioning between amphibole, phlogopite, and basanite melt: Earth and Planetary Science Letters, v. 135, p. 13–30.doi: 10.1016/0012-821X(95)00146-4

Le Maitre, R.W., 1989, A classification of igneous rocks and Glossary of Terms: Blackwell Recommendations of the International Union of Geological Sciences Subcommission on the Systematics of Igneous Rocks, 193 p p.

Liu, J., Sun, H., Wang, Z., Xia, Q., and Li, W., 2019, Continuous water supply from the subducted pacific plate to the Eastern Asian big mantle wedge: New insights from the water content of late Cretaceous OIB-like basalts: Lithos, p. 105–249. doi: 10.1016/j.lithos.2019.105249

McDonough, W.F., and Frey, F.A., 1989, REE in upper mantle rocks. In: Geochemistry and mineralogy of rare Earth elements: Mineralogical Society of America, v. 21, p. 99–145.

McKenzie, D.P., and O'Nions, R.K., 1991, Partial melt distributions from inversion of rare earth element concentrations: Journal of Petrology, v. 32, p. 1027–1091.doi: 10.1093/petrology/32.5.1021

Moghadam, H., Griffin, W.L., Kirchenbaur, M., Garbe-Schönberg, D., Zakie Khedr, M., Kimura, J.I., Stern, R.J., Ghorbani, G., Murphy, R., O'Reilly, S.Y., and Arai, S., 2018, Roll-back, extension and mantle upwelling triggered eocene potassic magmatism in NW Iran: Journal of Petrology, v. 59, p. 1417–1465.doi: 10.1093/petrology/egy067

Moghadam, H., Li, X.H., Ling, X.X., Santos, J.F., Stern, R.J., Li, Q.L., and Ghorbani, G., 2015, Eocene Kashmar granitoids (NE Iran): Petrogenetic constraints from U–Pb zircon geochronology and isotope geochemistry: Lithos, v. 216, p. 118–135.doi: 10.1016/j.lithos.2014.12.012

Muñoz, J.B., and Stern, C.R., 1989, Alkaline magmatism within the segment 38°–39° S of the Plio-Quaternary volcanic belt of the Southern South American Continental Margin: Journal of Geophysical Research: Solid Earth, v. 94, p. 4545–4560.doi: 10.1029/JB094iB04p04545

Nielsen, R.L., Ustunisik, G., Weinsteiger, A.B., Tepley III, F.J., Johnston, A.D., and Kent, A.J., 2017, Trace element partitioning between plagioclase and melt: An investigation of the impact of experimental and analytical procedures: Geochemistry, Geophysics, Geosystems, v. 18, no. 9. p. 3359–3384.doi: 10.1002/2017GC007080

Nouri, F., Azizi, H., Stern, R.J., Asahara, Y., Khodaparast, S., Madanipour, S., and Yamamoto, K., 2018, Zircon U-Pb dating, geochemistry and evolution of the Late Eocene Saveh magmatic complex, central Iran: Partial melts of sub-continental lithospheric mantle and magmatic differentiation: Lithos, v. 314, p. 274–292.doi: 10.1016/j.lithos.2018.06.013

Omrani, J., Agard, P., Whitechurch, H., Benoit, M., Prouteau, G., and Jolivet, L., 2008, Arc-magmatism and subduction history beneath the Zagros Mountains, Iran: A new report of adakites and geodynamic consequences: Lithos, v. 106, p. 380–398.doi: 10.1016/j.lithos.2008.09.008

Pang, K.N., Chung, S.L., Zarrinkoub, M.H., Lin, Y.C., Lee, H.Y., Lo, C.H., and Khatib, M.M., 2013, Iranian ultrapotassic volcanism at~ 11 Ma signifies the initiation of post-collisional magmatism in the A rabia–E urasia collision zone: Terra Nova, v. 25, p. 405–413.doi: 10.1111/ter.12050

Pearce, J.A., 2008, Geochemical fingerprinting of oceanic basalts with applications to ophiolite classification and the search for Archean oceanic crust: Lithos, v. 100, p. 14–48.doi: 10.1016/j.lithos.2007.06.016

Pearce, J.A., Harris, N.B., and Tindle, A.G., 1984, Trace element discrimination diagrams for the tectonic interpretation of granitic rocks: Journal of Petrology, v. 25, p. 956–983.doi: 10.1093/petrology/25.4.956

Pearce, J.A., and Norry, M.J., 1979, Petrogenetic implications of Ti, Zr, Y, and Nb variations in volcanic rocks: Contributions to Mineralogy and Petrology, v. 69, p. 33–47.

Pearce, J.A., and Stern, R.J., 2006, Origin of back-arc basin magmas: Trace element and isotope perspectives: Geophysical Monograph-American Geophysical Union, v. 166, p. 63.doi: 10.1029/166GM06

Pilet, S., Baker, M.B., and Stolper, E.M., 2008, Metasomatized lithosphere and the origin of alkaline lavas: Science, v. 320, p. 916–919.doi: 10.1126/science.1156563

Plank, T., and Langmuir, C.H., 1998, The chemical composition of subducting sediment and its consequences for the crust and mantle: Chemical Geology, v. 145, p. 325–394.doi: 10.1016/S0009-2541(97)00150-2

Prelević, D., Akal, C., Romer, R.L., and Foley, S.F., 2010, Lamproites as indicators of accretion and/or shallow subduction in the assembly of south-Western Anatolia, Turkey: Terra Nova, v. 22, p. 443–452.doi: 10.1111/j.1365-3121.2010.00963

Qiu, X.L., Zhao, M.H., Ao, W., Lu, C.C., Hao, T.Y., You, Q.Y., Ruan, A.G., and Li, J.B., 2011, OBS survey and crustal structure of the Southwest Sub-basin and Nansha Block, South China Sea: Diqiu Wuli Xuebao, v. 54, p. 3117–3128.

Ramezani, J., and Tucker, R.D., 2003, The Saghand region, central Iran: U-Pb geochronology, petrogenesis and implications for Gondwana tectonics: American Journal of Science, v. 303, p. 622–665.doi: 10.2475/ajs.303.7.622

Rehkamper, M., and Hofmann, A.W., 1997, Recycled ocean crust and sediment in Indian Ocean MORB: Earth and Planetary Science Letters, v. 147, p. 93–106.doi: 10.1016/S0012-821X(97)00009-5

Rezaei-Kahkhaei, M., Galindo, C., Pankhurst, R.J., and Esmaeily, D., 2011, Magmatic differentiation in the calc-alkaline Khalkhab–Neshveh pluton, Central Iran: Journal of Asian Earth Sciences, v. 42, p. 499–514.doi: 10.1016/j.jseaes.2011.04.022

Rudnick, R.L., and Fountain, D.M., 1995, Nature and composition of the continental-crust: A lower crustal perspective: Reviews of Geophysics, v. 33, p. 267–309.doi: 10.1029/95RG01302

Saccani, E., 2015, A new method of discriminating different types of post-Archean ophiolitic basalts and their tectonic significance using Th-Nb and Ce-Dy-Yb systematics: Geoscience Frontiers, v. 6, p. 481–501.doi: 10.1016/j.gsf.2014.03.006

Sarjoughian, F., Kananian, A., Haschke, M., and Ahmadian, J., 2012, Geochemical signature of Eocene Kuh-e Dom shoshonitic dikes in NE Ardestan, Central Iran: Implications for melt evolution and tectonic setting: Journal of Geosciences, v. 57, p. 241–264.doi: 10.3190/jgeosci.126

Shervais, J.W., 2001, Birth, death, and resurrection: The life cycle of suprasubduction zone ophiolites: Geochemistry, Geophysics, Geosystems, v. 2, no. 1, (2000GC000080). doi:10.1029/2000GC000080

Sokol, K., Prelević, D., Romer, R.L., Božović, M., van den Bogaard, P., Stefanova, E., Kostić, B., and Čokulov, N., 2019, Cretaceous ultrapotassic magmarism from the Sava-Vardar zone of the Balkans: Lithos, p. 105–268. doi: 10.1016/j.lithos.2019.105268

Stöcklin, J., 1968, Structural history and tectonics of Iran, a review: American Association of Petroleum Geologists, v. 52, p. 1229–1258.

Sun, S.S., and McDonough, W.F., 1989, Chemical and isotopic systematic of oceanic basalts: Implication for mantle composition and processes, Sunders, A.D., and Norry, M.J., eds., Magmatic in oceanic Basins: R Publications, Vol. 42, 313–345 p. doi: 10.1144/GSL.SP.1989.042.01.19

Takahashi, T., Hirahara, Y., Miyazaki, T., Senda, R., Chang, Q., Kimura, J.I., and Tatsumi, Y., 2012, Primary magmas at the volcanic front of the NE Japan arc: Coeval eruption of crustal low-K tholeiitic and mantle-derived medium-K calc-alkaline basalts at Azuma volcano: Journal of Petrology, v. 54, p. 103–148.doi: 10.1093/petrology/egs065

Tanaka, T., Togashi, S., Kamioka, H., Amakawa, H., Kagami, H., Hamamoto, T., Yuhara, O., Yoneda, Y., Shimizu, S., Kunimaru, H., Takahashi, T., Yanagi, K., Nakano, T., Fugimaki, H., Shinjo, R., Asahara, Y., Tanimizu, M., and Dragusanu, C., 2000, JNdi-1: A neodymium isotopic reference in consistency with La Jolla neodymium: Chemical Geology, v. 168, p. 279–281.doi: 10.1016/S0009-2541(00)00198-4

Taylor, S.R., and Mclennan, S.M., 1985, The continental crust: Its composition and evolution: Blackwell Scientific Publication, Oxford.

Temizel, I., Arslan, M., Yücel, C., Abdioğlu, E., and Ruffet, G., 2016, Geochronology and geochemistry of Eocene-aged volcanic rocks around the Bafra (Samsun, N Turkey) area: Constraints for the interaction of lithospheric mantle and crustal melts: Lithos, v. 258, p. 92–114.doi: 10.1016/j.lithos.2016.04.023

Torabi, G., 2009, Subduction-related eocene shoshonites from the cenozoic Urumieh-Dokhtar magmatic arc (Qaleh-Khargooshi area, Western Yazd Province, Iran): Turkish Journal of Earth Sciences, v. 18, p. 583–613.

Tutti, F., Yazdani, S., and Bazargani-Guilani, K., 2008, Geochemistry and petrogenesis of an alkaline-calc alkaline volcanic suite north Central Iran: The role of crystal fractionation and enrichment processes in a back-arc environment: Scientific Quarterly Journal, Geosciences, v. 67, p. 210–223.*(in Persian)*

Verdel, C., Wernicke, B.P., Hassanzadeh, J., and Guest, B., 2011, A Paleogene extensional arc flare-up in Iran: Tectonics, v. 30, p. 3008–3302.doi: 10.1029/2010TC002809

Vogel, T.A., Patino, L.C., Eaton, J.K., Valley, J.W., Rose, W.I., Alvarado, G.E., and Viray, E.L., 2006, Origin of silicic magmas along the Central American volcanic front: Genetic relationship to mafic melts: Journal of Volcanology and Geothermal Research, v. 156, p. 217–228.doi:10.1016/j.jvolgeores.2006.03.002

Walker, J.A., 1981, Petrogenesis of lavas from cinder cone fields behind the volcanic front of Central America: The Journal of Geology, v. 89, p. 721–739.doi: 10.1086/628638

Walter, M.J., 1998, Melting of garnet peridotite and the origin of komatiite and depleted lithosphere: Journal of Petrology, v. 39, p. 29–60.doi: 10.1093/petroj/39.1.29

Wang, C., Ding, L., Zhang, L.Y., Kapp, P., Pullen, A., and Yue, Y.H., 2016, Petrogenesis of Middle–Late Triassic volcanic rocks from the Gangdese belt, southern Lhasa terrane: Implications for early subduction of Neo-Tethyan oceanic lithosphere: Lithos, v. 262, p. 320–333.doi: 10.1016/j.lithos.2016

Whitney, D.L., and Evans, B.W., 2010, Abbreviations for names of rock forming minerals: American Mineralogist, v. 95, p. 77–185.doi: 10.2138/am.2010.3371

Wilson, A.H., Zeh, A., and Gerdes, A., 2017, In situ Sr isotopes in plagioclase and trace element systematics in the lowest part of the Eastern Bushveld Complex: Dynamic processes in an evolving magma Chamber: Journal of Petrology, v. 58, no. 2. p. 327–360.doi: 10.1093/petrology/egx018

Wilson, M., 2007, Igneous Petrogenesis: Chapman & Hall, London, 466 p p.

Wilson, M., and Patterson, R., 2001, Intraplate magmatism related to short-wavelength convective instabilities in the upper mantle: Evidence from the Tertiary-Quaternary volcanic province of western and central Europe: Special Paper of the Geological Society of America, v. 352, p. 37–58.doi: 10.1130/0-8137-2352-3.37

Winchester, J.A., and Floyd, P.A., 1977, Geochemical discrimination of different magma series and their differentiation products using immobile elements: Chemical Geology, v. 20, p. 325–343.doi:10.1016/0009-2541(77)90057-2

Workman, R.K., Hart, S.R., Jackson, M., Regelous, M., Farley, K.A., Blusztajn, J., Kurz, M., and Staudigel, H., 2004, Recycled metasomatized lithosphere as the origin of the Enriched Mantle II (EM2) end-member: Evidence from the Samoan Volcanic Chain: Geochemistry, Geophysics, Geosystems, v. 5, no. 4. doi:10.1029/2003GC000623

Xia, Y., Xu, X., Niu, Y., and Liu, L., 2018, Neoproterozoic amalgamation between Yangtze and Cathaysia blocks: The magmatism in various tectonic settings and continent-arc-continent collision: Precambrian Research, v. 309, p. 56–87. doi: 10.1016/j.precamres.2017.02.020

Xu, Z., Han, B.F., Ren, R., Zhou, Y.Z., Zhang, L., Chen, J.F., Su, L., Li, X.H., and Liu, D.Y., 2012, Ultramafic–mafic mélange, island arc and post-collisional intrusions in the Mayile Mountain, West Junggar, China: Implications for Paleozoic intra-oceanic subduction–accretion process: Lithos, v. 132, p. 141–161.doi: 10.1016/j.lithos.2011.11.016

Yazdani, S., Castillo, P., and Day, J., 2014, The geochemistry of zeolites and calc alkaline rocks from north-central Iran and its implications to fluid/rock interaction and alteration: SIO Student Symposium: University of California, San Diego.

Yazdani, S., Castillo, P.R., and Hassanzadeh, J., 2018, Crust-mantle interaction inferred from the petrology and Sr-Nd-Pb isotope geochemistry of Eocene arc lavas from the Kahrizak Mountains, north-central Iran: Lithos, v. 318, p. 299–313.doi: 10.1016/j.lithos.2018.08.018

Yoshida, T., 2001, The evolution of arc magmatism in the NE Honshu arc, Japan: Tohoku Geophysical Journal, v. 36, p. 131–149.

Yücel, C., Arslan, M., Temizel, I., Yazar, E.A., and Ruffet, G., 2017, Evolution of K-rich magmas derived from a net veined lithospheric mantle in an ongoing extensional setting: Geochronology and geochemistry of Eocene and Miocene volcanic rocks from Eastern Pontides (Turkey): Gondwana Research, v. 45, p. 65–86.doi: 10.1016/j.gr.2016.12.016

Zamanni, P., and Hossaini, H., 1999, Geological Map of Qom: Geology Survey of Iran, scale 1:100000, NO. 6159 doi:10.1046/j.1469-1809.1999.6320101.x

Zhao, Z., Mo, X., Dilek, Y., Niu, Y., DePaolo, D.J., Robinson, P., Zhu, D., Sun, C., Dong, G., Zhou, S., and Luo, Z., 2009, Geochemical and Sr–Nd–Pb–O isotopic compositions of the post-collisional ultrapotassic magmatism in SW Tibet: Petrogenesis and implications for India intra-continental subduction beneath southern Tibet: Lithos, v. 113, p. 190–212.doi: 10.1016/j.lithos.2009.02.004

Zheng, R., Wu, T., Zhang, W., Xu, C., and Meng, Q., 2013, Late Paleozoic subduction system in the southern Central Asian orogenic belt: Evidences from geochronology and geochemistry of the Xiaohuangshan ophiolite in the Beishan orogenic belt: Journal of Asian Earth Sciences, v. 62, p. 463–475.doi: 10.1016/j.jseaes.2012.10.033

Zheng, Y.F., and Hermann, J., 2014, Geochemistry of continental subduction-zone fluids: Earth, Planets and Space, v. 66, p. 93.doi: 10.1186/1880-5981-66-93

Zindler, A., and Hart, S., 1986, Chemical geodynamics: An. Rev. Earth and Planetary Sciences, v. 14, p. 493–571.doi:10.1146/annurev.ea.14.050186.002425

Zindler, A., Staudigel, H., and Batiza, R., 1984, Isotope and trace element geochemistry young Pacific seamounts: Implications for the scale of upper mantle heterogeneity: Earth and Planetary Science Letters, v. 70, p. 175–195.doi: 10.1016/0012-821X(84)90004-9